JCB Journal of Cell Biology

ARTICLE

Local regulation of extracellular vesicle traffic by the synaptic endocytic machinery

Cassandra R. Blanchette[1*], Amy L. Scalera[1*], Kathryn P. Harris[2,3], Zechuan Zhao[1], Erica C. Dresselhaus[1], Kate Koles[1], Anna Yeh[1], Julia K. Apiki[1], Bryan A. Stewart[2,3], and Avital A. Rodal[1]

Neuronal extracellular vesicles (EVs) are locally released from presynaptic terminals, carrying cargoes critical for intercellular signaling and disease. EVs are derived from endosomes, but it is unknown how these cargoes are directed to the EV pathway rather than for conventional endolysosomal degradation. Here, we find that endocytic machinery plays an unexpected role in maintaining a release-competent pool of EV cargoes at synapses. Endocytic mutants, including *nervous wreck* (*nwk*), *shibire*/dynamin, and *AP-2*, unexpectedly exhibit local presynaptic depletion specifically of EV cargoes. Accordingly, *nwk* mutants phenocopy synaptic plasticity defects associated with loss of the EV cargo synaptotagmin-4 (Syt4) and suppress lethality upon overexpression of the EV cargo amyloid precursor protein (APP). These EV defects are genetically separable from canonical endocytic functions in synaptic vesicle recycling and synaptic growth. Endocytic machinery opposes the endosomal retromer complex to regulate EV cargo levels and acts upstream of synaptic cargo removal by retrograde axonal transport. Our data suggest a novel molecular mechanism that locally promotes cargo loading into synaptic EVs.

Introduction

Neurons depend on complex and highly interconnected endosomal membrane trafficking pathways to sort physiologically and pathologically relevant cargoes (Winckler et al., 2018; Yarwood et al., 2020). One function of endosomal trafficking in neurons is to sort cargoes for release in extracellular vesicles (EVs; Blanchette and Rodal, 2020). EVs are small membrane-bound compartments that transport protein, lipid, and nucleic acid cargoes from EV-releasing cells to target cells (van Niel et al., 2018). In the nervous system, EV-mediated cargo transport regulates intercellular communication and contributes to neurodegenerative disease pathology (Budnik et al., 2016; Holm et al., 2018; Song et al., 2020). However, our understanding of how EV cargo traffic is spatially and temporally regulated within the polarized and complex morphology of neurons remains limited (Blanchette and Rodal, 2020).

Exosomes are a type of EV generated when endosomal multivesicular bodies (MVBs) undergo fusion with the plasma membrane to release their intralumenal vesicles. Alternatively, MVBs can be trafficked to the lysosome for cargo degradation (van Niel et al., 2018). It remains unclear how and where MVBs are generated in neurons, and how they are directed to an EV versus lysosomal fate. We previously described a trafficking pathway that controls the levels of EV cargoes in donor neuron synaptic terminals, regulated by endosome-plasma membrane recycling machinery including the retromer complex and Rab11 (Walsh et al., 2021). This suggests the existence of a specialized presynaptic "EV-permissive" recycling compartment, where cargo is protected from degradation en route to MVB formation and released from donor cells. However, the mechanisms by which this compartment is loaded are unknown.

The *Drosophila* larval neuromuscular junction (NMJ) is a powerful in vivo model for addressing the gaps in our understanding of synaptic EV biology (Ashley et al., 2018; Koles et al., 2012; Korkut et al., 2009; Korkut et al., 2013; Lauwers et al., 2018; Walsh et al., 2021). EVs are released from the presynaptic terminals of larval motor neurons and accumulate postsynaptically within the folds of the muscle membrane subsynaptic reticulum (SSR) or are taken up by muscles and glia (Fuentes-Medel et al., 2009; Koles et al., 2012). EVs released at the *Drosophila* NMJ likely represent exosomes, as presynaptic terminals contain MVBs positive for EV cargoes and release EVs similar in size to exosomes (Koles et al., 2012; Korkut et al., 2009; Walsh et al., 2021). Several endogenously and exogenously expressed transmembrane proteins have been characterized as neuronal EV cargoes at the *Drosophila* NMJ, including synaptotagmin-4 (Syt4), which drives functional and structural plasticity, as

[1]Department of Biology, Brandeis University, Waltham, MA; [2]Department of Biology, University of Toronto Mississauga, Mississauga, Canada; [3]Department of Cell and Systems Biology, University of Toronto, Toronto, Canada.

*C.R. Blanchette and A.L. Scalera contributed equally to this paper. Correspondence to Avital A. Rodal: arodal@brandeis.edu.

well as the Alzheimer's disease-associated human amyloid precursor protein (hAPP; Korkut et al., 2013; Walsh et al., 2021). Thus, the *Drosophila* NMJ provides a unique opportunity to interrogate the mechanisms and functional significance of traffic of EV cargoes in an intact nervous system. Here, using this system, we have identified a novel and unexpected role for canonical endocytic machinery in locally maintaining EV cargoes in EV-permissive compartments at synaptic terminals, thereby promoting their release in synaptically derived EVs. Our work suggests that endocytic machinery regulates endosomal sorting in neurons to protect EV cargoes from retrograde transport-mediated depletion at synaptic terminals.

Results

EV cargoes are locally depleted at *nwk* mutant presynaptic terminals

EVs at the *Drosophila* larval NMJ are derived from neuronal membranes, and thus contain neuronal glycoproteins that can be detected using α-HRP antibodies (Fuentes-Medel et al., 2009; Snow et al., 1987; Walsh et al., 2021). During our studies of the endocytic FCH-BIN amphiphysin RVS (F-BAR) and SH3 domain-containing protein Nervous Wreck (Nwk), we found that *nwk* null mutants exhibited a strong reduction in the intensity of postsynaptic α-HRP puncta (within 3 µm of the boundary of motor neurons innervating muscles 6 and 7; Fig. 1 A). This suggests that in addition to its previously defined roles in synaptic morphogenesis, growth factor receptor trafficking, endocytosis, and synaptic transmission (Coyle et al., 2004; Del Signore et al., 2021; O'Connor-Giles et al., 2008; Rodal et al., 2008; Ukken et al., 2016), Nwk may also regulate EV cargo traffic at synapses.

α-HRP antibodies are likely to detect many neuronal proteins undergoing a variety of trafficking itineraries (Snow et al., 1987), only a small fraction of which result in EV sorting. Therefore, we next tested the role of *nwk* in the traffic of specific established EV cargoes. First, using endogenously tagged Syt4-GFP (Walsh et al., 2021), we found that loss of *nwk* led to reduced mean postsynaptic Syt4-GFP levels, together with a decreased number of postsynaptic Syt4-GFP puncta (Fig. 1 B), similar to the α-HRP signal. Using this single, defined cargo, we also detected a striking reduction presynaptically (Fig. 1 B), which was surprising since endocytic mutants would be expected to accumulate cargoes at the plasma membrane. These phenotypes were rescued by neuronal re-expression of Nwk using the binary GAL4/UAS (upstream activating sequence) system (Fig. 1 B). Taken together, these results suggest that Nwk cell autonomously regulates Syt4 levels in EV donor neurons, resulting in reduced release of Syt4 in EVs. Loss of *nwk* similarly caused a dramatic decrease in pre- and postsynaptic levels of several other known EV cargoes, including neuronal GAL4-driven hAPP (hAPP-EGFP [enhanced GFP]; Walsh et al., 2021), the neuronal GAL4-driven long isoform of evenness interrupted (Evi) tagged with EGFP (Evi-EGFP; Korkut et al., 2009), and the endogenous neuronal isoform of neuroglian (Nrg; Walsh et al., 2021; Fig. 1 C and Fig. S1, A–C). This phenotype was not specific to muscle 6/7, as we observed a similar effect at the NMJ on muscle 4 (Fig. 1 C; and Fig. S1, D and E). Therefore, the effects of *nwk* mutants are consistent for multiple neurons and EV cargoes. These observations highlight a new role for Nwk in regulating the levels of EV cargo proteins in donor synapses, and thus in the recipient postsynaptic cell.

To test if this effect was specific to EV cargoes, we measured the presynaptic levels of two transmembrane proteins that are not normally trafficked into EVs: the calcium sensor synaptotagmin-1 (Syt1), which is associated with synaptic vesicles (Littleton et al., 1993), and the bone morphogenetic protein (BMP) signaling receptor thickveins (Tkv), which localizes to the plasma membrane and endosomes (Deshpande et al., 2016; Smith et al., 2012). We found that presynaptic levels of both endogenous Syt1 and neuronally GAL4-driven UAS-Tkv-mCherry were similar between *nwk* mutants and controls (Fig. 1, D and E), suggesting that reduction of Syt4, hAPP, Evi, and Nrg in *nwk* mutants is specific to the EV trafficking itinerary.

We next asked whether Nwk functions to maintain EV cargo levels specifically at synaptic terminals or throughout the neuron. We measured the mean intensity of Syt4-GFP in the cell bodies and dendrites within the larval ventral nerve cord, and the mean intensity of hAPP-EGFP (as the Syt4-GFP signal was too faint for this analysis) in the region of the motor neuron axon closest to muscle 4 synaptic terminals. We found that *nwk* mutants had similar levels of Syt4-GFP in cell bodies and dendrites compared to controls, and similar levels of hAPP-EGFP in their axons compared to controls (Fig. 1 F). We next used live imaging to ask whether *nwk* mutants exhibit defects in the velocity or directionality of EV cargo transport in axons. We found no change in the dynamics of hAPP-EGFP puncta in *nwk* mutant axons compared to controls (Fig. S1, F–H), suggesting that changes to axonal transport are unlikely to account for the depletion of EV cargoes we observed at *nwk* mutant synaptic terminals. Together, these results suggest that Nwk specifically and locally regulates the levels of EV cargo proteins at synapses.

nwk mutants phenocopy loss of EV cargo function

We next asked if depletion of EV cargoes at *nwk* mutant synapses causes a loss of EV cargo function. At the NMJ, traffic of Syt4 into EVs is thought to regulate multiple forms of activity-dependent synaptic growth and plasticity (Barber et al., 2009; Harris et al., 2018; Korkut et al., 2013; Piccioli and Littleton, 2014; Yoshihara et al., 2005). In this system, high-frequency stimulation causes an increase in the frequency of miniature excitatory junction potentials (mEJPs). This functional plasticity is termed high-frequency stimulation-induced miniature release (HFMR) and depends on presynaptically derived Syt4 (Korkut et al., 2013). To directly test whether *nwk* mutants exhibit a loss of Syt4 function and, therefore, phenocopy *syt4* mutant defects, we measured the responses of *nwk* mutant synapses to high-frequency stimulation, and found that HFMR was strongly reduced in *nwk* mutants (Fig. 2, A–C), similar to *syt4* mutants (Yoshihara et al., 2005). This phenotype could be rescued by neuronal but not muscle GAL4-driven expression of Nwk, indicating that HFMR specifically requires presynaptic Nwk (Fig. 2 C).

We next tested whether Nwk is required for Syt4-dependent structural plasticity. Spaced potassium stimulation of wild-type

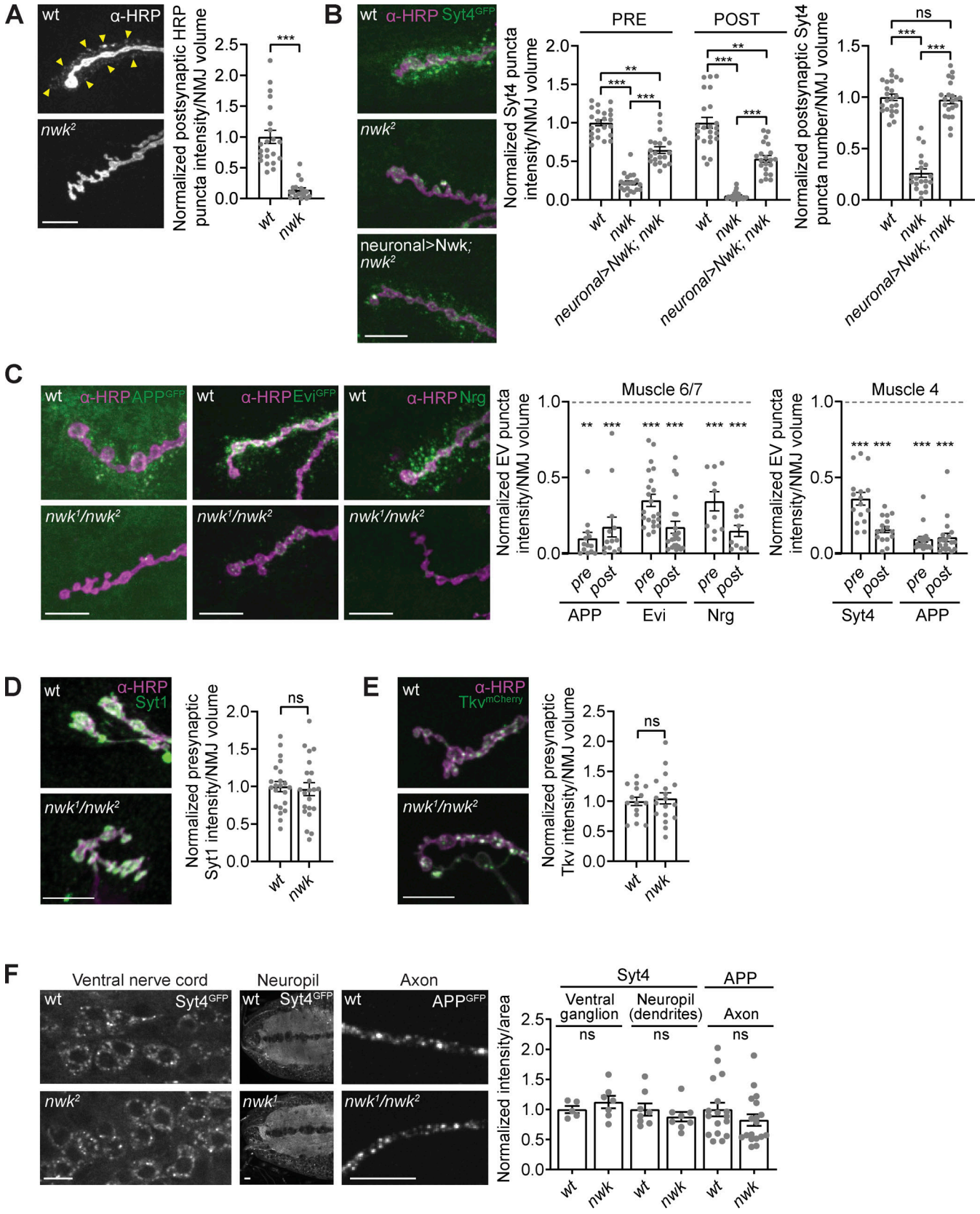

Figure 1. **EV cargoes are locally depleted at *nwk* mutant synapses. (A)** *nwk* mutant synapses lack α-HRP–labeled postsynaptic neuronal membrane puncta (indicated by arrowheads). Left: Representative images of muscle 6/7 NMJs. Right: Quantification of postsynaptic α-HRP puncta intensity. **(B)** *nwk* mutants cause neuron-autonomous pre- and postsynaptic depletion of the endogenously tagged EV cargo Syt4-GFP. Nwk was expressed using C380-GAL4, a neuron-specific driver. Left: Representative images of muscle 6/7 NMJs. Right: Quantification of Syt4-GFP puncta intensity and number. **(C)** EV cargoes APP-GFP,

Evi-GFP, Nrg, and Syt4-GFP are reduced at *nwk* mutant synapses. Left: Representative images of muscle 6/7 NMJs. Middle: Quantification of EV cargo puncta intensity at muscle 6/7. Right: Quantification of EV cargo puncta intensity at muscle 4. Dashed line indicates mean EV cargo levels at control NMJs. **(D and E)** Levels of the non-EV cargoes Syt1 and Tkv-mCherry are unaffected at *nwk* mutant synapses. Left: Representative images of muscle 6/7 NMJs (Syt1) and muscle 4 NMJs (Tkv-mCherry). Right: Quantification of Syt1 or Tkv-mCherry puncta intensity. **(F)** EV cargo levels remain unchanged in cell bodies, neuropil, and axons in *nwk* mutants. Left: Representative images of Syt4-GFP in ventral ganglion cell bodies and neuropil, and APP-GFP in axons. Right: Quantification of Syt4-GFP or APP-GFP intensity. Data is represented as mean ± SEM; *n* is depicted by individual gray dots on the graphs and represents NMJs (A–E), or axons or brains (F). NMJ intensity measurements were normalized to presynaptic volume; all measurements were further normalized to the mean of their respective controls. All scale bars are 10 µm. Associated with Fig. S1. See Table S1 and Table S3 for detailed genotypes, sample sizes, and statistical analyses. wt, wild-type.

Drosophila synapses leads to the Syt4-dependent formation of nascent synapses, termed ghost boutons, which contain presynaptic markers but have not yet assembled postsynaptic components such as Discs Large (Dlg; Ataman et al., 2008; Korkut et al., 2013; Piccioli and Littleton, 2014). In contrast to the significant increase in ghost bouton formation following spaced stimulation in control animals, *nwk* mutants did not show an increase (Fig. 2 D). Together, these results indicate that *nwk* mutants exhibit a loss of Syt4 function in activity-dependent synaptic growth and plasticity. Since *nwk* mutants have normal Syt4 levels in cell bodies and neuropil, these results further suggest that Syt4 specifically requires presynaptic localization for its functions.

As loss of *nwk* led to a decrease in hAPP at NMJs (Fig. 1 C and Fig. S1, A and E), we tested if loss of *nwk* correlates with a reduction in hAPP-induced toxicity. GAL4-mediated neuronal overexpression of hAPP and the amyloidogenic protease beta secretase (BACE) leads to defects including decreased eclosion (Chakraborty et al., 2011; Greeve et al., 2004; Mhatre et al., 2014; Fig. 2 E). Remarkably, this eclosion defect was significantly suppressed in both *nwk* heterozygous and *nwk* homozygous mutant backgrounds, suggesting that loss of even one copy of *nwk* can reduce the toxicity of hAPP and BACE in the adult nervous system (Fig. 2 E). The suppression was not due to broad changes in hAPP levels in adult fly head protein extracts, again suggesting a local and specific effect (Fig. 2 F). Together these results show that the depletion of EV cargoes Syt4 and hAPP at *nwk* mutant synaptic terminals correlates with a loss of function for these EV cargos in the nervous system.

Endocytic machinery regulates EV cargo traffic at synapses

Nwk is a conserved membrane-remodeling protein that physically interacts with components of the canonical clathrin-associated endocytic machinery (Almeida-Souza et al., 2018; Del Signore et al., 2021; O'Connor-Giles et al., 2008; Rodal et al., 2008; Xiao et al., 2018; Xiao and Schmid, 2020). At *Drosophila* synapses, this machinery controls synaptic vesicle recycling, synaptic transmission, and growth factor receptor trafficking (Deshpande and Rodal, 2015; Kaempf and Maritzen, 2017). We hypothesized that like Nwk, other endocytic proteins may also regulate EV cargo traffic at synapses. We therefore investigated EV cargo traffic in mutants of endocytic proteins of diverse functions including regulation of membrane lipid composition, membrane remodeling, and the cytoskeleton. Loss of the lipid phosphatase synaptojanin (Synj) or presynaptic knockdown of the endocytic adapter Dap160/intersectin led to a depletion of Syt4-GFP both pre- and postsynaptically (Fig. 3 A; and Fig. S2, A and B). Further, neuronal expression of a dominant negative dynamin mutant (Shi^{K44A}) or presynaptic knockdown of the membrane-deforming protein Endophilin A (EndoA) caused reduction of postsynaptic α-HRP puncta (Fig. 3 B; and Fig. S2, D and E). By contrast, both pre- and postsynaptic Syt4-GFP levels were slightly increased in null mutants of the BAR-SH3 sorting nexin SH3PX1/Snx9, despite its physical interaction with Nwk (Ukken et al., 2016; Fig. 3 A and Fig. S2 C). These results indicate that maintenance of EV cargo levels at synapses is a function shared by some but not all Nwk-interacting endocytic machinery.

The canonical function of endocytic proteins is to control clathrin-mediated endocytosis, which is a primary mechanism for synaptic vesicle recycling at the *Drosophila* larval NMJ (Heerssen et al., 2008; Kasprowicz et al., 2008) and is required for synaptic morphogenesis via endocytic traffic of growth factor receptors (Choudhury et al., 2016; Dwivedi et al., 2021). We asked if clathrin and its heterotetrameric AP-2 adaptor complex were similarly involved in synaptic EV cargo traffic. We found that mutants lacking the AP-2σ subunit exhibited a significant decrease in pre- and postsynaptic levels of Syt4-GFP (Figs. 4 A and S3 A). Surprisingly, we found mutants lacking either the AP-2α or the AP-2µ subunit exhibited only a mild decrease in presynaptic levels of Syt4-GFP, and no significant change postsynaptically (Figs. 4 A and S3 B). This suggests that the levels of EV cargo at synapses specifically depend on the AP-2σ subunit, or that there is redundancy between the AP-2α and AP-2µ subunits, as has been previously suggested (Gu et al., 2013). To decipher between these possibilities, we measured Syt4-GFP levels in *AP-2α; AP-2µ* double mutants and found a striking decrease in pre- and postsynaptic levels of Syt4-GFP, similar to *nwk* mutants (Figs. 4 A and S3 B). Thus, EV cargo levels are dependent on the AP-2 clathrin adaptor complex with functional redundancies among the AP-2α and AP-2µ subunits.

The importance of the AP-2 clathrin adaptor complex in EV cargo regulation prompted us to test directly whether EV cargo levels at synapses are dependent on clathrin itself. We examined Syt4-GFP in hypomorphic mutants of clathrin light chain (*clc*) or clathrin heavy chain (*chc*). We found no change in presynaptic levels of Syt4-GFP in *clc* and *chc* mutants compared to controls, but its localization was drastically shifted into large α-HRP–positive presynaptic accumulations (Fig. 4, B and C; and Fig. S3, C and D). This change in Sy4-GFP presynaptic localization in *clc* and *chc* mutants was associated with a striking decrease in postsynaptic levels of Syt4-GFP compared to controls (Fig. 4 B; and Fig. S3, C and D), suggesting that Syt4-GFP is not released in EVs from clathrin mutant synapses. The inactivation of clathrin is known to lead to the formation of large cisternal membrane compartments derived from bulk membrane

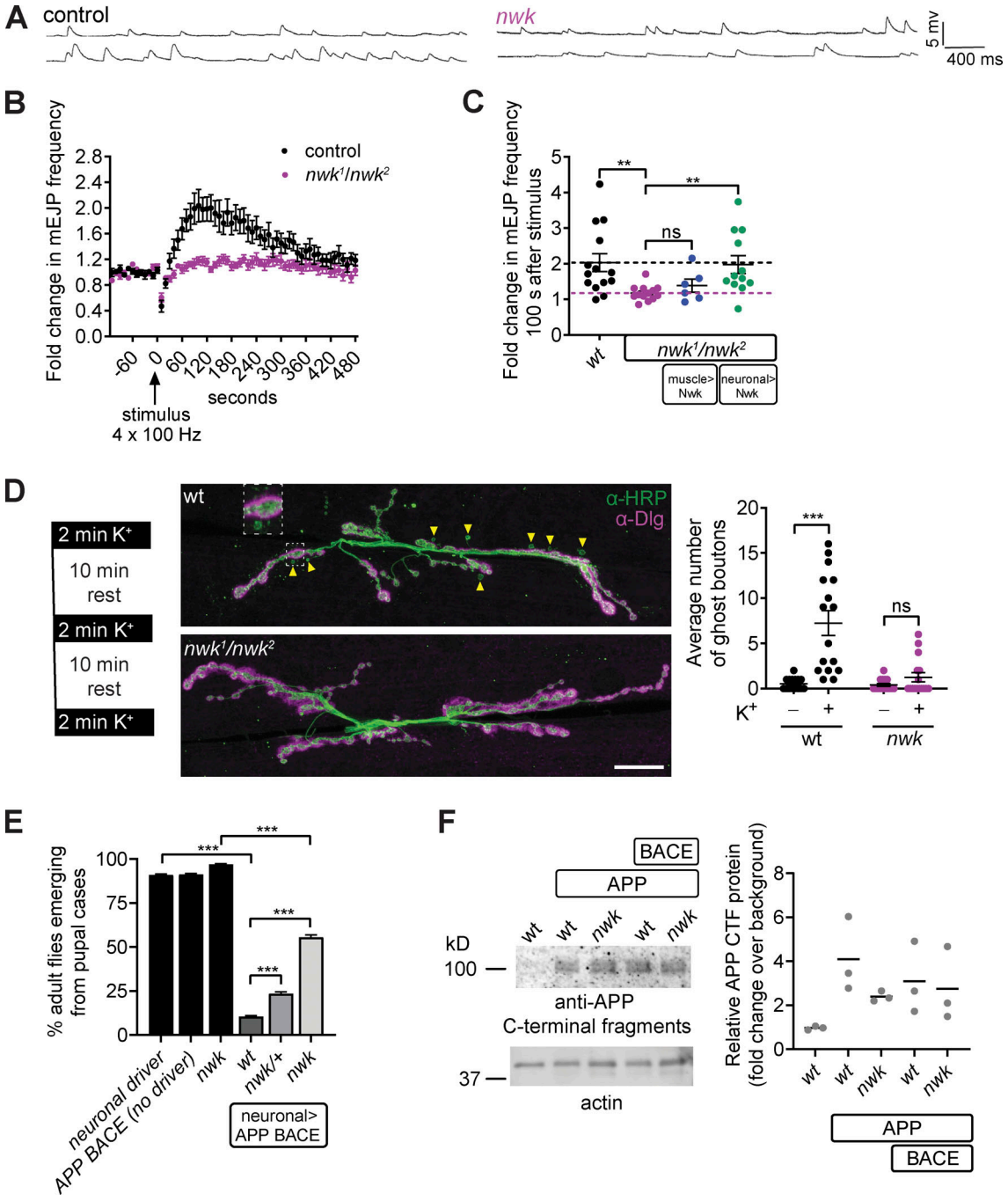

Figure 2. ***nwk* mutants exhibit loss of EV cargo function. (A–C)** Syt4-dependent functional plasticity (HFMR) is abolished in *nwk* mutants. **(A)** Representative traces of mEJPs before (top trace) and after (bottom trace) high-frequency stimulation (4 × 100 Hz). (**B**) Timecourse of mEJP frequency after stimulation. **(C)** *nwk* mutant HFMR phenotype is cell autonomous to neurons. Scatter plot of mEJP frequency 100 s after high-frequency stimulation. Black dashed line represents wild-type (*wt*) mean value, and the pink dashed line represents *nwk* mean value. C57-GAL4 and Vglut-GAL4 are muscle and neuron-specific drivers, respectively. **(D)** Syt4-dependent structural plasticity (ghost bouton budding) is abolished in *nwk* mutants. Left: Paradigm for spaced stimulation with high K^+/Ca^{2+}. Middle: Representative maximum intensity projections of confocal stacks at muscle 6/7 labeled with α-HRP (presynaptic) and α-Dlg (postsynaptic) antibodies. Arrowheads point to ghost boutons, containing HRP but not Dlg, enlarged in inset. Scale bar is 20 µm. Right: Quantification of ghost boutons with and without stimulation. **(E)** APP BACE-induced eclosion defect is suppressed in *nwk* mutants. Graph shows the percentage of adult flies emerging from pupal cases. APP and BACE were expressed with C155-GAL4, a neuron-specific driver. **(F)** $GAL4^{C155}$-driven APP levels are comparable in wt and *nwk* heads: Immunoblot of *Drosophila* head extracts with α-APP C-terminal fragment and α-actin antibodies. Quantification shows fold change of APP relative to actin levels. Data is represented as mean ± SEM (B, C, and D) or mean ± standard error of the proportion (E); *n* represents NMJs (B–D), pupal cases (E), or biological replicates (F), and in C, D, and F, *n* is depicted by individual gray dots on the graphs. See Table S1 and Table S3 for detailed genotypes, sample sizes, and statistical analyses. Source data are available for this figure: SourcedataF2.

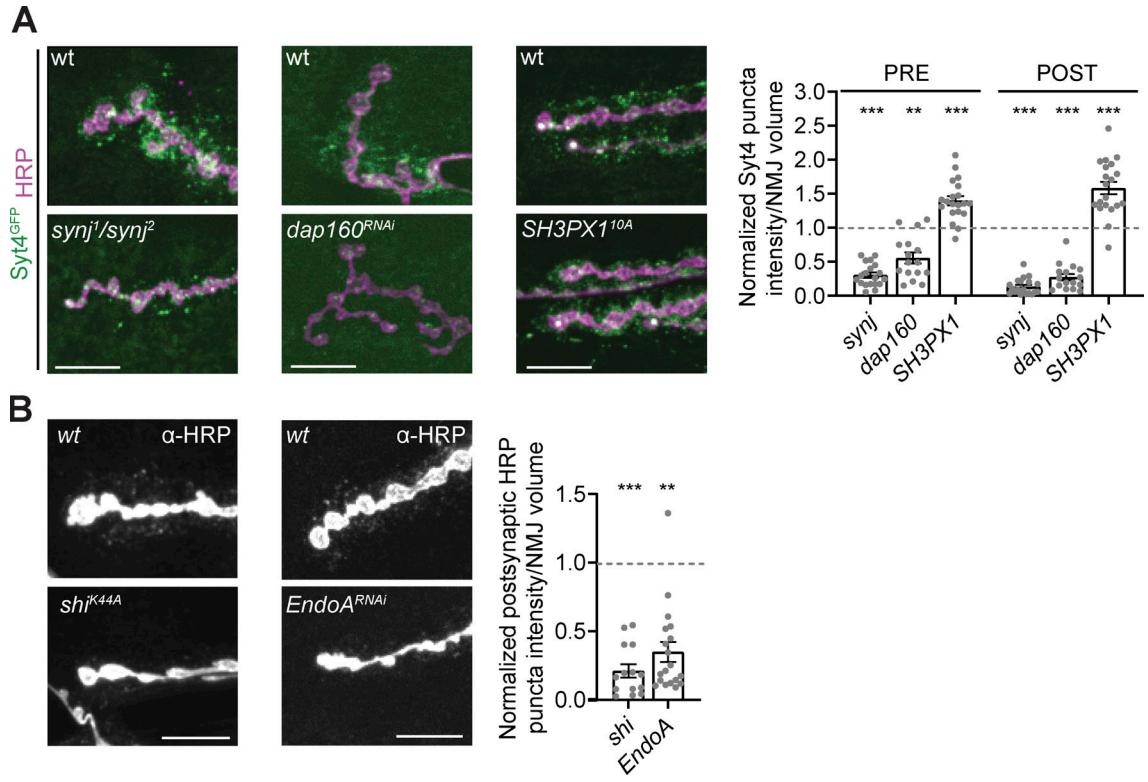

Figure 3. **A subset of endocytic machinery is required for EV cargo trafficking.** Pre- and postsynaptic EV cargo levels are reduced in multiple endocytic mutants. **(A)** Left: Representative images of muscle 6/7 NMJs. Right: Quantification of Syt4-GFP puncta intensity. **(B)** Left: Representative images of α-HRP debris on muscle 6/7 NMJs. Right: Quantification of α-HRP debris intensity. Data is represented as mean ± SEM; *n* is depicted by individual gray dots on the graphs and represents NMJs. NMJ intensity measurements were normalized to presynaptic volume; all measurements were further normalized to the mean of their respective controls, which are indicated with a dashed line. All scale bars are 10 µm. Associated with Fig. S2. See Table S1 and Table S3 for detailed genotypes, sample sizes, and statistical analyses. wt, wild-type.

uptake in synapses (Heerssen et al., 2008; Kasprowicz et al., 2008), which may correspond to the Syt4-GFP and HRP-positive accumulations that we see in *clc* and *chc* synapses. As *nwk* mutants exhibit a significant depletion of EV cargoes both pre- and postsynaptically (Fig. 1, B and C), we wondered whether these presynaptic accumulations of Syt4-GFP in *clc* and *chc* mutants would be sensitive or resistant to loss of *nwk*. We found that simultaneous loss of *clc* and *nwk* phenocopied loss of *clc* alone with regards to levels and localization of Syt4-GFP pre- and postsynaptically (Fig. 4 D). This suggests that the Syt4-GFP accumulations in *clc* mutant synapses are not accessible to the mechanism by which EV cargoes are depleted at *nwk* mutant synapses. Although the grossly disrupted membrane structures found at clathrin mutant synaptic terminals make it difficult to interpret the specific role of clathrin itself in EV cargo traffic, our finding that loss of canonical clathrin adaptors recapitulates the phenotypes of other endocytic mutants suggests that a clathrin-associated mechanism regulates maintenance of EV cargoes at synapses.

Nwk opposes the function of Vps35/retromer in EV cargo trafficking

We next explored the mechanisms by which Nwk-associated membrane-remodeling machinery controls the distribution of EV cargoes between release in EVs versus synaptic depletion. One possibility is that this machinery acts at the plasma membrane in a noncanonical role to regulate fusion of EV-containing MVBs (similar to functions of dynamin at chromaffin granule fusion pores (Anantharam et al., 2011; Wong et al., 2015) and that in its absence these MVBs are targeted for degradation. Alternatively, endocytic machinery could serve a canonical function in endocytic loading of cargoes into an EV-permissive precursor compartment that populates MVBs destined for EV release. Mutation of the retromer complex component *Vps35* causes accumulation of EV cargoes in these precursor compartments and a concomitant increased release of EVs (Walsh et al., 2021). If the Nwk-dependent endocytic machinery acts to promote EV fusion with the plasma membrane, we would expect to see recovery of presynaptic cargo levels in *Vps35; nwk* double mutants relative to *nwk* single mutants, but reduced postsynaptic recovery, as MVBs would not be released (Fig. 5 A, "release"). On the other hand, if Nwk plays a more canonical role in loading MVB precursors prior to their release, we would expect to see recovery of both pre- and postsynaptic EV cargo levels in *Vps35; nwk* mutants relative to *nwk* single mutants (Fig. 5 A, "sorting"). We found that loss of *Vps35* in the *nwk* mutant background significantly increased Syt4-GFP levels both pre- and postsynaptically, and also significantly increased the number of postsynaptic Syt4-GFP puncta (Fig. 5 B) compared to the *nwk* mutant alone, suggesting that Nwk is involved in loading EV precursors and

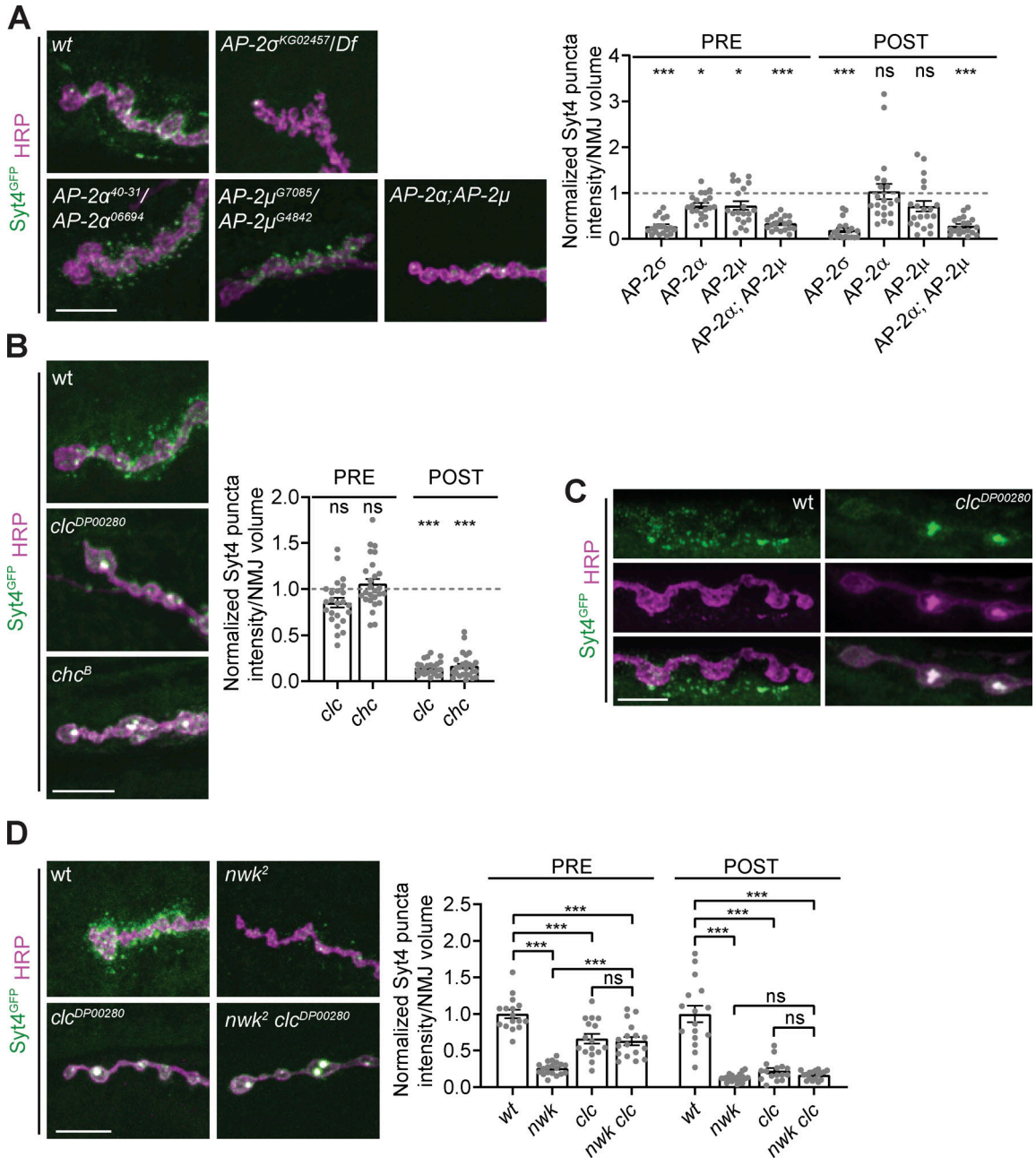

Figure 4. **EV cargo trafficking requires clathrin-associated endocytic machinery. (A)** Pre- and postsynaptic EV cargo levels are reduced in clathrin adaptor AP-2 mutants. Left: Representative images of muscle 6/7 NMJs. Right: Quantification of Syt4-GFP puncta intensity. **(B)** EV cargoes show altered localization in clathrin mutants and are not released from neurons. Left: Representative images of muscle 6/7 NMJs. Right: Quantification of Syt4-GFP puncta intensity. **(C)** Airyscan microscopy of *clc* mutant muscle 6/7 NMJs show that EV cargo accumulations extend into the interior of the bouton. **(D)** EV cargo accumulation in clathrin mutants is epistatic to its depletion in *nwk* mutants. Left: Representative images of muscle 6/7 NMJs. Right: Quantification of Syt4-GFP puncta intensity. Data is represented as mean ± SEM; *n* is depicted by individual gray dots on the graphs and represents NMJs. NMJ intensity measurements were normalized to presynaptic volume; all measurements were further normalized to the mean of their respective controls, which is indicated with a dashed line. All scale bars are 10 µm. Associated with Fig. S3. See Table. S1 and Table. S3 for detailed genotypes, sample sizes, and statistical analyses. wt, wild-type.

maintaining presynaptic cargo levels, rather than in fusion of MVBs and release of EVs from the neuron.

Nwk acts upstream of dynactin-mediated retrograde transport

Our data suggest that endocytic machinery protects EV cargoes from degradation by loading them into an EV-permissive precursor compartment. We hypothesized that in *nwk* mutants, these EV cargoes may be depleted from the synapse via retrograde traffic to the cell body for lysosomal degradation. To test this, we overexpressed a dominant negative dynactin (DCTN) truncated p150/Glued subunit to inhibit dynein/dynactin-mediated retrograde transport (Allen et al., 1999). In otherwise wild-type synapses expressing DCTN-p150$^{\Delta}$, we found that

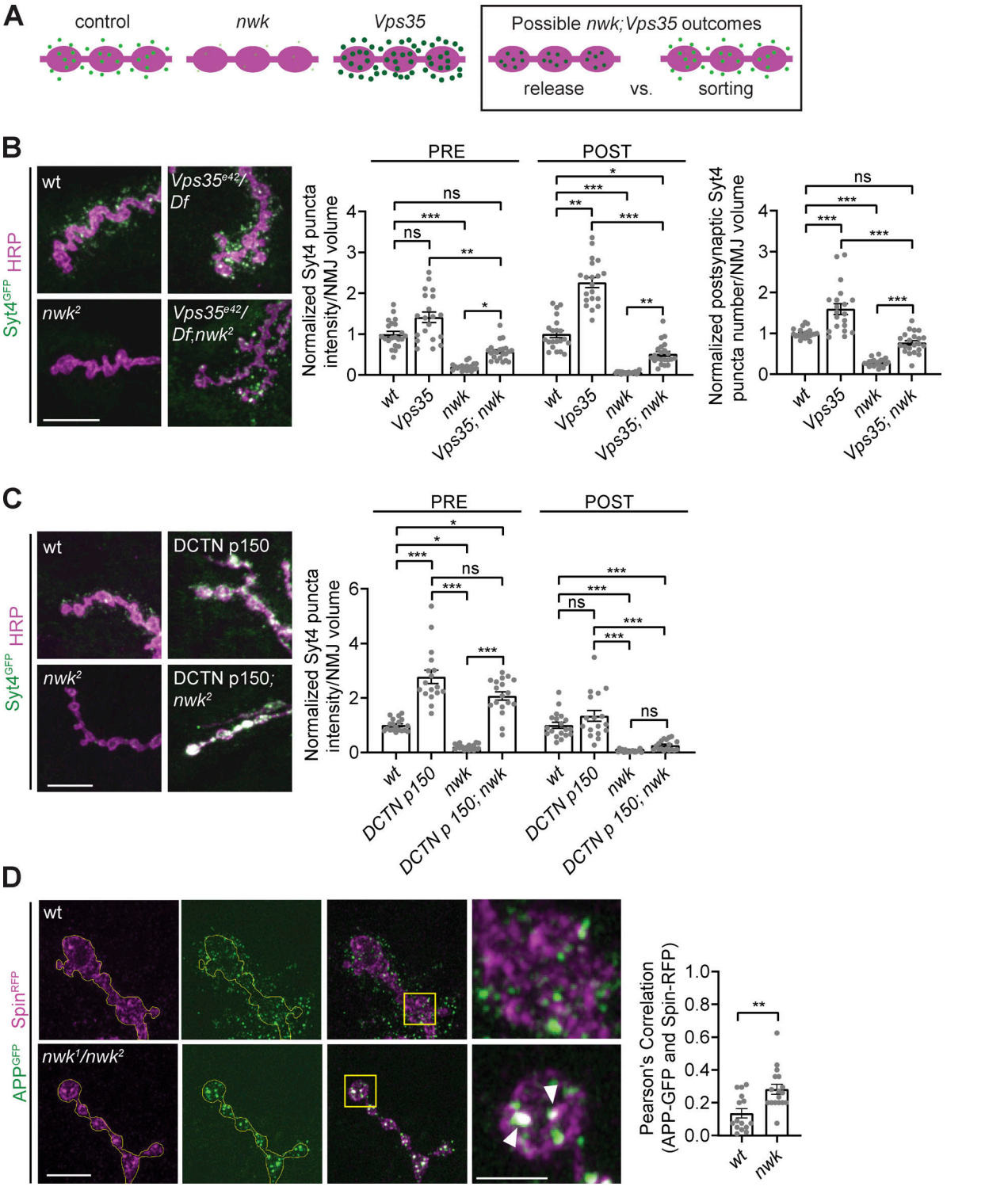

Figure 5. **Nwk opposes retromer in loading EV precursors and acts upstream of dynactin-mediated retrograde transport. (A)** Cartoon depicting potential EV phenotype outcomes for *nwk; Vps35* experiment, testing if Nwk regulates MVB–plasma membrane fusion or EV cargo sorting. **(B)** EV cargoes are increased both pre- and postsynaptically in *nwk; Vps35* double mutants relative to *nwk* mutants. Left: Representative images of muscle 6/7 NMJs. Right: Quantification of Syt4-GFP puncta intensity and number. **(C)** EV cargoes are retained at the synapse upon p150-DCTN overexpression, but these compartments are not competent for EV release. Left: Representative images of muscle 6/7 NMJs. Right: Quantification of Syt4-GFP puncta intensity. **(D)** EV cargo APP-GFP exhibits enhanced colocalization with the late endosome/lysosome marker Spin in *nwk* mutants. Left: Airyscan microscopy of muscle 6/7 NMJs. Outlines of presynaptic region are shown in yellow. Middle: Zoom of boutons of yellow boxed regions of NMJ. Arrowhead points to colocalized spots of APP-GFP and Spin-RFP. Right: Pearson's correlation of APP-GFP and Spin-RFP signal within the presynaptic region only. Data is represented as mean ± SEM; *n* is depicted by individual gray dots on the graphs and represents NMJs. NMJ intensity measurements were normalized to presynaptic volume; all measurements were further normalized to the mean of wild-type (wt) controls. Scale bars are 10 µm (B and C), 5 µm (D, three rows of panels on left), and 2 µm (D, enlarged insets on right). Associated with Fig. S4. See Table S1 and Table S3 for detailed genotypes, sample sizes, and statistical analyses.

presynaptic Syt4-GFP levels more than doubled (Fig. 5 C), indicating that EV cargoes do undergo retrograde transport and build up at the synapse in the absence of dynein-mediated transport. Interestingly, there was no concomitant increase in postsynaptic Syt4-EGFP levels (Fig. 5 C), indicating that the cargoes destined for retrograde transport are located in a non-EV permissive compartment. We then used this system to test whether in *nwk* mutants EV cargoes are depleted from the synapse due to retrograde transport. We overexpressed DCTN-p150$^{\Delta}$ in the *nwk* mutant background and found the same striking increase in presynaptic Syt4-GFP levels as in wild-type synapses (Fig. 5 C). This result both provides further evidence that delivery of EV cargoes to synapses is not compromised in *nwk* mutants and indicates that they are largely being depleted from synapses by retrograde transport. Further, postsynaptic Syt4-GFP levels remained low relative to wild-type controls (Fig. 5 C), indicating that in *nwk* mutants synaptic EV cargoes that are destined for retrograde transport are in a non-EV permissive compartment.

To explore the nature of this compartment, we examined presynaptic colocalization of EV cargoes with the late endosome/lysosome marker Spinster (Spin; Sweeney and Davis, 2002). Expression of Spin-RFP did not modify the *nwk* mutant EV phenotype at synaptic terminals, as we still observed a pre- and postsynaptic depletion of hAPP-EGFP (Fig. S4 A). Notably, the residual hAPP-EGFP puncta in *nwk* mutant presynaptic terminals exhibited increased colocalization with Spin-RFP compared to controls (Fig. 5 D), with no change in colocalization with the presynaptic membrane-marking α-HRP signal as a negative control (Fig. S4 B), indicating that EV cargoes are shifted to degradative compartments in *nwk* mutants. Finally, we observed a mild decrease in Spin-RFP intensity at *nwk* mutant NMJs (Fig. S4 C), indicating that degradative compartments are not expanded in these mutant synapses, and further suggesting that sorting defects occur upstream of endolysosomal maturation. Overall, our data suggest a working model in which synaptic depletion of EV cargoes in *nwk* mutants results from a shift of cargoes toward a degradative compartment that cannot produce EVs and is sent to the cell body via retrograde transport (Fig. 6).

Discussion

Here we report a novel function of canonical endocytic machinery in regulating trafficking of EV cargoes at synapses in vivo. We find that endocytic mutants exhibit a local depletion of EV cargoes at synaptic terminals, correlating with a loss of Syt4-dependent synaptic plasticity at the larval NMJ and a reduction in APP-dependent toxicity in the adult nervous system. Mechanistically, the endocytic machinery opposes the retromer complex in sorting cargoes into EV-precursor compartments and acts upstream of dynactin-mediated retrograde transport. Together, our data support a working model in which the endocytic machinery protects EV cargoes from local depletion at synaptic terminals, consequently preserving cargo function and promoting its release in EVs. Our results suggest a new interpretation for previously reported phenotypes of endocytic mutants and uncover a new pathway for investigating and therapeutically intervening in EV traffic.

EV traffic is genetically separable from canonical functions of the endocytic machinery

Our discovery that EV cargoes are depleted from endocytic mutant synaptic terminals was surprising, as the expected phenotype for loss of endocytic machinery is accumulation of EV cargoes at the plasma membrane. Indeed, the phenotypes we observed for endocytic mutants (reduction in cargo levels) and retromer (increase in cargo levels; Walsh et al., 2021) at synapses are opposite to what has been found for EV-relevant cargoes in other cell types. For example, in several *Caenorhabditis elegans* cell types, Wntless/Evi accumulates near the plasma membrane in *dpy-23*/AP-2 mutants and is depleted in *vps-35* mutants (Pan et al., 2008; Yang et al., 2008). Similarly, EV cargoes are trapped at the plasma membrane upon inhibition of endocytosis in PC12 cells and sympathetic neuronal cell bodies (Escudero et al., 2014), or in HeLa cells (Janvier and Bonifacino, 2005; Lau and Chou, 2008). Our results underscore the unique properties of trafficking in distal neuronal processes such as synapses, due to their extreme morphology and limited lysosomal capacity, and highlight the importance of using in vivo models to study neuronal EVs (Blanchette and Rodal, 2020; Ferguson, 2018).

Our new findings also add to the diverse functions of the endocytic machinery in neurons, including synaptic vesicle recycling, release site clearance, synaptic transmission, signaling receptor trafficking, and synaptic growth (Chanaday et al., 2019; Deshpande and Rodal, 2015). If EV cargo trafficking defects in endocytic mutants were indirectly caused by impairment of these canonical roles, then we would expect the severity of EV phenotypes to consistently scale with defects in these other functions. However, we find that mutants with more severe defects in synaptic vesicle recycling (e.g., *AP-2α*; Gonzalez-Gaitan and Jackle, 1997) exhibit very mild EV phenotypes, while mutants with mild synaptic vesicle cycling phenotypes (e.g., *nwk* and *dap160*; Del Signore et al., 2021; Koh et al., 2004; Marie et al., 2004) have severe EV defects. In a similar vein, *AP-2α*, *AP-2μ*, and *dap160* mutants exhibit severe synaptic growth phenotypes (Choudhury et al., 2016; Dwivedi et al., 2021; Koh et al., 2004; Marie et al., 2004), likely due to the failure to downregulate BMP receptor signaling (Deshpande and Rodal, 2015). Among these, only loss of *dap160* has a severe EV defect. By contrast, *nwk* mutants have a relatively mild synaptic growth phenotype (Coyle et al., 2004) and a severe EV phenotype. *Vps35*/retromer mutants also exhibit synaptic vesicle cycling defects (Inoshita et al., 2017) and BMP pathway-dependent synaptic overgrowth (Korolchuk et al., 2007), but conversely accumulate excess EV cargoes rather than depleting them (Walsh et al., 2021). Thus, synaptic vesicle endocytosis, synaptic growth signaling, and EV trafficking can be genetically uncoupled.

EV trafficking functions of the endocytic machinery are also unlikely to arise from indirect effects on neurotransmitter release. For example, loss of *EndoA* leads to decreased EV cargo levels, but *EndoA* mutants have no defects in synaptic transmission (Verstreken et al., 2002). Interestingly, *nwk* and *SH3PX1*

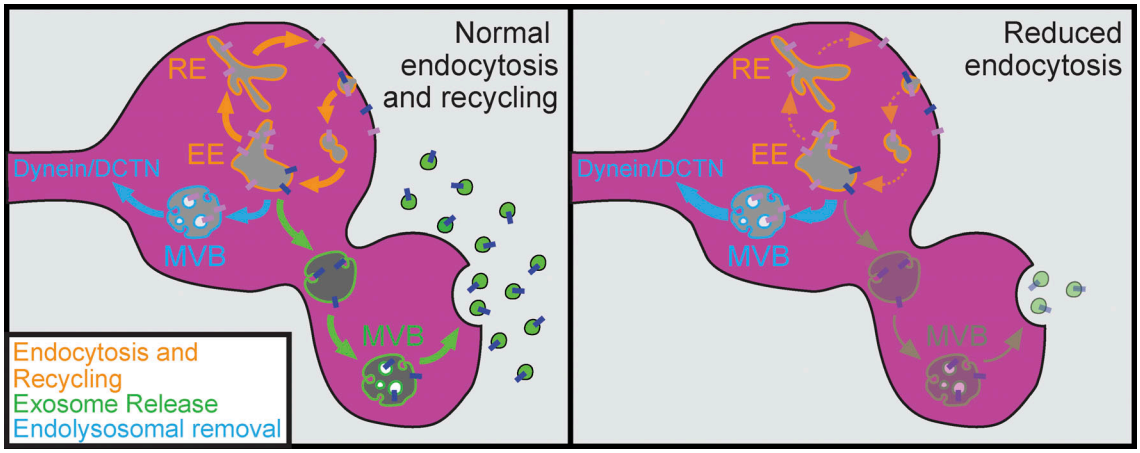

Figure 6. **Endocytic machinery protects EV cargoes from local synaptic depletion.** At wild-type synapses, proper traffic and function of EV cargoes depend on a robust flux through the recycling pathway (left, orange arrows). However, endocytic mutant synapses exhibit a depletion of EV cargoes, likely due to reduced recycling flux, resulting in aberrant sorting for degradation upstream of dynactin/dynein mediated retrograde transport (right). EE is early endosome, RE is recycling endosome.

physically interact and share a role in synaptic transmission (Cao et al., 2013; Coyle et al., 2004; Ukken et al., 2016). However, this shared role is not linked to their EV functions, as we found that *SH3PX1* mutants exhibit a significant increase in EV cargo levels, opposite to *nwk* mutants. SH3PX1 could directly inhibit the EV cargo sorting activity of Nwk, or else it may act independently on recycling endosomes to restrict EV traffic, as suggested by studies of its functions in other cell types (Bendris and Schmid, 2017; Knaevelsrud et al., 2013; Zhang et al., 2019). Overall, our results indicate that the role of endocytic machinery in regulating EV cargo traffic is genetically separable from its roles in synaptic transmission, synaptic vesicle endocytosis, and synaptic growth, and instead reflects an independent and novel function of these conserved molecules at synaptic terminals.

Endocytic machinery sorts cargoes into EV-precursor compartments

What then is the mechanism by which endocytic machinery regulates EV cargo levels? Our data indicate that Nwk functions in an opposing pathway to the retromer complex to load cargoes into EV-permissive compartments. One possibility is that this occurs via the canonical role of the clathrin/AP-2 endocytic machinery at the plasma membrane (Kaksonen and Roux, 2018). Our data differentiating the phenotypes of clathrin and AP-2 mutants provide some insights into the specific mechanisms involved: We find that clathrin is strictly required to form functional EV precursors, and in its absence, cargoes likely accumulate in large cisternae. By contrast, loss of AP-2 adaptors and other endocytic machinery leads to cargo depletion, perhaps due to a slowed but still partially functional endocytic pathway (Chen and Schmid, 2020; Dickman et al., 2005). Indeed, efficient endocytic internalization could be required for effective EV loading by increasing the flux of cargo through the endosome–plasma membrane recycling pathway that populates these EV precursor compartments (Walsh et al., 2021; Fig. 6, orange arrows). In support of this hypothesis, loss of *nwk* phenocopies mutation of the recycling endosome regulator Rab11, including presynaptic depletion of EV cargoes in opposition to retromer, and loss of Syt4 physiological function (Ashley et al., 2018; Koles et al., 2012; Korkut et al., 2013; Walsh et al., 2021). Finally, our observation that AP-2α and AP-2μ exhibit partial redundancy indicates that hemicomplexes of AP-2 may be sufficient to sort EV cargo (Gu et al., 2013), or that other adaptors such as AP180 may also function in this pathway (Bao et al., 2005).

Alternatively, endocytic machinery may be acting in a non-canonical role on intracellular compartments to sort EV cargoes. Endocytic proteins are required to reform synaptic vesicles from endosomal intermediates, particularly during elevated activity (Heerssen et al., 2008; Kasprowicz et al., 2008; Kasprowicz et al., 2014; Kittelmann et al., 2013; Kononenko et al., 2014; Watanabe et al., 2014). Clathrin localizes directly to endosomes, where it regulates endosomal cargo sorting and intralumenal vesicle formation (Raiborg et al., 2001; Raiborg et al., 2006; Sachse et al., 2002; Shi et al., 2009; Wenzel et al., 2018). Further, the mammalian Nwk homolog FCHSD2, in addition to its role at the internalization step of endocytosis (Almeida-Souza et al., 2018; Xiao et al., 2018), suppresses recycling and lysosomal degradation of signaling receptors (Xiao and Schmid, 2020). Retromer functions directly on endosomes and genetically opposes the functions of Nwk, suggesting that Nwk may also act on endosomes. The extreme density of endocytic machinery at synaptic membranes makes it difficult to detect a small endosomally localized fraction, although Nwk does exhibit partial colocalization with Rab11 (Rodal et al., 2008). Future studies will be necessary to discriminate between whether clathrin-mediated endocytic machinery indirectly loads EV-precursor endosomes via canonical endocytosis, or if it instead acts on them directly.

EV cargo sorting for release occurs upstream of retrograde transport

Our data provide new insights into the overall trafficking itineraries of neuronal EV cargoes. The following observations suggest that EV precursor compartments are locally loaded at

synapses by the endocytic machinery: (1) We observed no defect in retrograde or anterograde axonal traffic that could account for reduced synaptic levels. (2) Endocytic machinery is abundant and active at synaptic terminals, and endocytic mutants lead to local loss of EV cargoes at synapses. (3) Dynactin mutants cause synaptic accumulation of EV cargo-containing compartments, indicating that these compartments are generated at synapses.

Our data also indicate that once cargoes are destined for retrograde transport, they are no longer EV permissive, and therefore dynein-mediated transport does not regulate release (as has been hypothesized in other systems; Heisler et al., 2018). Indeed, trapping these compartments at *nwk* mutant synapses is sufficient to restore presynaptic levels of EV cargoes but does not allow the release of these cargoes from the neuron. Thus, Nwk-mediated cargo sorting occurs upstream of retrograde transport, and the missorted cargoes in the *nwk* mutant are no longer EV-competent and are destined for synaptic removal, likely for degradation in the cell body. In support of this, we find enhanced colocalization between residual EV cargo puncta and the late endosome/lysosome marker Spin at *nwk* mutant synaptic terminals. Degradative lysosomes are enriched in cell bodies relative to axons and synaptic terminals (Ferguson, 2018; Lie et al., 2021), and there is also evidence of local protein degradation along axons or at axon terminals (Farfel-Becker et al., 2019; Jin et al., 2018). Our data suggest for the first time that synaptic EV cargoes are degraded after transport rather than on-site, although we cannot exclude the possibility of separate pools of cargoes: Some that are locally degraded, and some that are targeted for retrograde transport. Future in vivo investigations focused on the role of retrograde trafficking machinery and their adaptors may yield insights into additional points by which neurons control degradation of EV cargoes at distinct subcellular locations (Heisler et al., 2018; van Niel et al., 2018).

Implications for the functions of neuronal EVs and for EV-directed disease therapies

Although there has been an explosion of research identifying the contents of EVs and the diverse functions of their cargoes, the field has been lacking approaches to specifically manipulate their biogenesis and release. Our findings provide new tools to ask where EV cargoes act in the neuron, to locally manipulate EV cargo levels at synapses, and to define the functions of the EV trafficking route. We found that loss of *nwk* leads to a local decrease in EV cargo levels presynaptically (and as a result, postsynaptically), with a corresponding loss of EV cargo function, indicating that levels of EV cargoes at synaptic terminals, but not elsewhere in the neuron, correlate with EV cargo function. Importantly, to date, endogenous EV cargo function at the *Drosophila* NMJ has not been tested in trafficking mutants that are demonstrated to specifically disrupt EV release without impacting levels in the donor cell (Ashley et al., 2018; Korkut et al., 2009; Korkut et al., 2013; Lauwers et al., 2018). Our results suggest that in addition to the trans-synaptic signaling functions that have been previously proposed, EV trafficking could play an equally important role for cargoes whose primary function is in the donor neuron, as a proteostatic mechanism to maintain levels at specific subcellular locations such as synapses.

Given that local depletion of EV cargoes at *nwk* mutant synapses correlates with a loss of their physiological functions, EV cargo misregulation may also play unrecognized roles in the previously reported phenotypes of endocytic mutants. These may therefore need to be reinterpreted in the context of local synaptic loss of a multitude of EV cargoes (Holm et al., 2018). For example, Shi^{ts} mutants have been used in numerous *Drosophila* circuit-mapping studies to block synaptic transmission at the restrictive temperature (Kitamoto, 2001); however, these mutants also show defects at the permissive temperature (Dickman et al., 2006), which could inadvertently cause chronic loss of EV cargoes important for that circuit. Further, neurological phenotypes of mice mutant for endocytic machinery could be consistent with EV signaling defects (Holm et al., 2018; Malakooti et al., 2020; Milosevic et al., 2011).

Finally, our results suggest new interpretations of neurological disease mechanisms. Defects in EV and endosomal trafficking are linked to neurodegenerative diseases such as Alzheimer's disease (Becot et al., 2020; Song et al., 2020; Winckler et al., 2018). Aged neurons exhibit increased APP endocytosis, leading to endosomal dysfunction and synapse loss (Burrinha et al., 2021). Our data predict that this may also promote APP loading into the EV pathway. This is consistent with previous reports suggesting that upregulation of endocytic machinery exacerbates Alzheimer's disease phenotypes (Keating et al., 2006; Ren et al., 2008; Yu et al., 2018), and that loss of endocytic machinery can suppress these phenotypes (Zhu et al., 2013). Downregulation of APP, either genetically or by enhancing lysosomal biogenesis, can suppress generation of amyloid beta and amyloid plaques in Alzheimer's disease (Hung et al., 2021; Xiao et al., 2015). We report a new and synapse-specific mechanism for targeting APP: Loss of *nwk* severely reduces synaptic levels of APP and ameliorates its toxicity in the nervous system while causing only mild defects in the synaptic vesicle cycle and synaptic growth. Our data suggest that therapeutically targeting EV-sensitive components of endocytic machinery could be a strategy to reduce pathological synaptic EV cargoes in neurological disease.

Materials and Methods

Drosophila culture

Flies were cultured using standard media and techniques. Flies used for experiments were maintained at 25°C, except for RNAi experiments (*Dap160* and *EndoA*) that were maintained at 29°C, and the chc^{B} and *clc nwk* experiments that were maintained at 20°C. For detailed information on fly stocks used, see Table S1, and for detailed genotype information for each figure panel, see Table S3.

Immunohistochemistry

Wandering third instar larvae from density-controlled crosses were dissected in HL3.1 (Feng et al., 2004) and fixed in HL3.1 with 4% paraformaldehyde for 10 min. For detailed information on antibodies used in this study, see Table S2. Washes and antibody dilutions were conducted using PBS containing 0.2% Triton X-100 (0.2% PBX). Primary antibody incubations were

conducted overnight at 4°C, and secondary antibody incubations for 1–2 h at room temperature. α-HRP incubations were conducted either overnight at 4°C or for 1–2 h at room temperature. Prior to imaging, fillets were mounted on slides with Vectashield (Vector Labs). α-GFP nanobodies (Nanotag Biotechnologies) were used to amplify Syt4-GFP signal only for Fig. 4 C.

Image acquisition and analysis

Image acquisition

For analysis of EV and non-EV cargoes, NMJs (muscle 6/7 [segments A2 and A3] and muscle 4 [segments A2, A3, and A4]), brains (neuropil and cell bodies), and axons were imaged at room temperature. Z-stacks were acquired using a Nikon Ni-E upright microscope equipped with a Yokogawa CSU-W1 spinning-disk head, an Andor iXon 897U EMCCD camera, and Nikon Elements AR software. A 60× (NA 1.4) oil immersion objective was used to image NMJs, cell bodies, and fixed axons, and a 40× (NA 0.75) oil immersion objective for neuropils. For axonal trafficking, timelapse images of axon bundles proximal to the ventral nerve cord were taken with a 60× (NA 1.4) oil immersion objective. Nine Z slices were collected per frame (Step size 0.3 µm, with no acquisition delay between timepoints, resulting in a frame rate of 2.34–2.37 s/frame). Airyscan images in Fig. 4 C and Fig. 5 D were acquired at room temperature with Zen Blue software on a Zeiss LSM880 Fast Airyscan microscope in super resolution acquisition mode, using a 63× (NA 1.4) oil immersion objective. Image acquisition settings were identical for all images in each independent experiment.

Quantification of pre- and postsynaptic EV cargo levels at the NMJ

The 3D volumetric analyses of pre- and postsynaptic EV cargoes at NMJs were carried out using Volocity 6.0 software (Perkin Elmer). For each NMJ image, both type 1s and 1b boutons were retained for analysis while axons were cropped out. Presynaptic volume was determined through manual thresholding to the α-HRP signal (excluding objects smaller than 7 μm^3 and closing holes), with a 3.3 µm dilation around this signal delineating the postsynaptic volume. Manual thresholding of the EV cargo signal was conducted to ensure measurements included only EV cargo signal above background muscle fluorescence. Postsynaptic objects smaller than 0.015 μm^3 were excluded. EV cargo sum intensity measurements were calculated within these pre- and postsynaptic volumes and normalized to the presynaptic volume. Puncta number was quantified only within the postsynaptic volume.

Quantification of Syt4-GFP in cell bodies

This analysis was conducted in FIJI. Syt4-GFP intensity in even-skipped positive motor neurons was measured from a single middle slice through each cell body. Mean Syt4-GFP intensity was calculated by subtracting the mean intensity of an area of background outside of the cell body in the same slice from the mean intensity within the manually selected cell body region. Each data point corresponds to the average mean Syt4-GFP intensity across eight cell bodies per brain.

Quantification of Syt4-GFP levels in neuropil

This analysis was conducted in FIJI. Using single slices through the center of the ventral ganglion, a region within the neuropil was manually selected. Mean Syt4-GFP intensity within this region of neuropil was calculated by subtracting the mean intensity of an area of background outside of the ventral ganglion from the mean intensity within the selected neuropil region.

Quantification of APP-EGFP levels in fixed axons

APP-EGFP levels were measured using FIJI in the m4 axon region between the segmental axon bundle and synaptic boutons. Average intensity projections were manually cropped to exclude everything aside from the axon segment to be measured. Manual thresholding to the HRP signal was conducted to determine the region for measurement. To calculate mean APP-EGFP intensity in the axon, the mean intensity of three areas of background per image were averaged and subtracted from the mean APP-EGFP intensity within the HRP-thresholded region.

Quantification of live axonal trafficking of APP-GFP puncta

To quantify APP-GFP dynamics in live axons, maximum intensity projections of time course images were processed in FIJI to subtract background and adjust for XY drift using the StackReg plugin. Kymographs were generated from one to four axons per animal using the FIJI plugin KymographBuilder. Kymographs were blinded, and a number of tracks were manually counted. The minimum track length measured was 3 µm, with most tracks above 5 µm. Velocity was measured by calculating the slope of the identified tracks.

Quantification of APP-GFP and Spin-RFP colocalization

This analysis was done in FIJI. A 3D presynaptic mask was created by combining signals of the presynaptically enriched labels α-HRP and Spin-RFP. To generate masks, images were subjected to a Gaussian blur and thresholded using the intensity of the combined channels. Specific parameters were optimized empirically and kept consistent between control and mutant groups. Colocalization analysis was performed on 3D Airyscan images using a FIJI script that utilizes the Coloc2 plugin for ImageJ (https://imagej.net/Coloc_2). Background was subtracted using the rolling ball method to a radius of 50 pixels. NMJ intensities were measured in Volocity as described above.

Western blot

Heads (15 pooled per genotype) from *Drosophila* aged 3–10 d were homogenized in 50 µl 2× Laemmli buffer. 15 µl of extract was loaded in each lane and fractionated by SDS/PAGE and immunoblotted with α-APP-CTF (A8717; Sigma-Aldrich) and α-actin (JLA-20; DHSB). Blots were visualized using a Biorad Chemidoc system and quantified using FIJI with APP-CTF values normalized to the corresponding actin loading control.

Eclosion assay

Density-controlled crosses were grown at 25°C for 17 d, and the number of eclosed and uneclosed pupal cases were counted for each genotype. Eclosion rate was calculated as the number of pupal cases eclosed divided by the total number of pupal cases.

Ghost bouton budding

Ghost bouton budding experiments were carried out as previously described (Piccioli and Littleton, 2014). Wandering third

instar larvae were dissected in HL3 saline solution (70 mM NaCl, 5 mM KCl, 0.2 $CaCl_2$, 20 mM $MgCl_2$, 10 mM $NaHCO_3$, 5 mM trehalose, 115 mM sucrose, and 5 mM Hepes-NaOH, pH 7.2). Larval dissections were matched to a guide with consistent dissection pin locations varying by 5%. The pins were moved inward to 60% of the original size of each larva. Relaxed fillets were incubated three times for 2 min in 90 mM K solution (40 mM NaCl, 90 mM KCl, 1.5 $CaCl_2$, 20 mM $MgCl_2$, 10 mM $NaHCO_3$, 5 mM trehalose, 5 mM sucrose, and 5 mM Hepes-NaOH, pH 7.2) spaced by 10 min in HL3 solution. After the third incubation, larvae were returned to HL3 solution and stretched to their original size. Ghost boutons were identified by the presence of a presynaptic bouton (HRP labeled) without the postsynaptic Dlg protein. Muscle 6/7 NMJs from segment 3 were included in analysis.

Electrophysiology

Wandering third instar larvae were dissected in HL3 saline (Stewart et al., 1994). Recordings were taken using an AxoClamp 2B amplifier (Axon Instruments). A recording electrode was filled with 3 M KCl and inserted into muscle 6 at abdominal segments A3 or A4. A stimulating electrode filled with saline was used to stimulate the severed segmental nerve using an isolated pulse stimulator (2100; A-M Systems). HFMR was induced by four trains of 100 Hz stimuli spaced 2 s apart in 0.3 mM extracellular Ca^{2+}. mEJPs were recorded 2 min before and 10 min after HFMR induction. mEJP frequency at indicated time points was calculated in 10-s bins. Fold enhancement was calculated by normalizing to the baseline mEJP frequency recorded prior to HFMR induction. Analyses were performed using Clampfit 10.0 software (Molecular Devices) and Mini Analysis 6.0.3 (Synaptosoft, Inc.). Each *n* value represents a single muscle recording, with data generated from at least six individual larvae of each genotype arising from at least two independent crosses. Resting membrane potentials were between −50 and −75 mV and were not different between genotypes. Input resistances were between 5 and 10 MΩ and were not different between genotypes.

Statistical analyses

All graphing and statistical analyses were completed using GraphPad Prism. Datasets were first analyzed with the D'Agostino-Pearson normality test. Normally distributed datasets were analyzed with either an unpaired two-sided *t*-test (two groups) or a one-way ANOVA with Tukey's multiple comparisons (more than two groups), while not normally distributed datasets were analyzed with either a two-sided Mann–Whitney test (two groups) or a Kruskal–Wallis test with Dunn's multiple comparisons (more than two groups). Error bars report ± SEM. The eclosion experiment in Fig. 2 E was analyzed using a chi-squared test; error bars report standard error of the proportion. Detailed information about genotypes, sample sizes, and statistical analyses performed for each dataset can be found in Table S3. *, P < 0.05; **, P < 0.01; ***, P < 0.001.

Online supplemental material

Fig. S1 shows source data for EV cargo levels at *nwk* mutant synapses and axonal transport measurements. Fig. S2 shows source data for EV cargo levels at endocytic mutant synapses. Fig. S3 shows source data for EV cargo levels at clathrin and clathrin adaptor mutant synapses. Fig. S4 shows controls for EV cargo localization to degradative compartments at *nwk* mutant synapses. Table S1 lists *Drosophila* strains. Table S2 lists antibodies and reagents. Table S3 lists statistics by dataset.

Acknowledgments

We thank the Bloomington *Drosophila* Stock Center (Indiana University, Bloomington, IN, NIH P40OD018537) and the Developmental Studies Hybridoma Bank created by the National Institute of Child Health and Human Development of the National Institutes of Health. We thank Kate O'Connor-Giles (Brown University, Providence, RI) and Vivian Budnik (UMass Chan Medical School, Worcester MA) for fly lines and Sultana Bhuiyan, Steven Del Signore, Jack Cheng, Biljana Ermanoska, and Matthew Pescosolido for technical assistance and helpful discussions.

This work was supported by National Institute of Neurological Disorders and Stroke grants R01 NS103967 to A.A. Rodal, F32 NS110123 to C.R. Blanchette, F32 NS120909 to E.C. Dresselhaus, and T32 MH019929 to A.L. Scalera, and by Natural Sciences and Engineering Research Council of Canada to B.A. Stewart (RGPIN-06004).

The authors declare no competing financial interests.

Author contributions: C.R. Blanchette, A.L. Scalera, and A.A. Rodal designed the study and experiments. C.R. Blanchette, A.L. Scalera, K.P. Harris, Z. Zhao, E.C. Dresselhaus, K. Koles, A. Yeh, and J.K. Apiki conducted the experiments and performed analyses. C.R. Blanchette, A.L. Scalera, and A.A. Rodal wrote the manuscript. C.R. Blanchette, A.L. Scalera, K.P. Harris, Z. Zhao, E.C. Dresselhaus, K. Koles, A. Yeh, J.K. Apiki, B.A. Stewart, A.A. Rodal reviewed and/or edited the manuscript. B.A. Stewart and A.A. Rodal provided supervision.

Submitted: 17 December 2021
Revised: 14 February 2022
Accepted: 28 February 2022

References

Allen, M.J., X. Shan, P. Caruccio, S.J. Froggett, K.G. Moffat, and R.K. Murphey. 1999. Targeted expression of truncated glued disrupts giant fiber synapse formation in *Drosophila*. *J. Neurosci.* 19:9374–9384. https://doi.org/10.1523/JNEUROSCI.19-21-09374.1999

Almeida-Souza, L., R.A.W. Frank, J. Garcia-Nafria, A. Colussi, N. Gunawardana, C.M. Johnson, M. Yu, G. Howard, B. Andrews, Y. Vallis, and H.T. McMahon. 2018. A flat BAR protein promotes actin polymerization at the base of clathrin-coated pits. *Cell*. 174:325–337.e14. https://doi.org/10.1016/j.cell.2018.05.020

Anantharam, A., M.A. Bittner, R.L. Aikman, E.L. Stuenkel, S.L. Schmid, D. Axelrod, and R.W. Holz. 2011. A new role for the dynamin GTPase in the regulation of fusion pore expansion. *Mol. Biol. Cell*. 22:1907–1918. https://doi.org/10.1091/mbc.E11-02-0101

Ashley, J., B. Cordy, D. Lucia, L.G. Fradkin, V. Budnik, and T. Thomson. 2018. Retrovirus-like gag protein Arc1 binds RNA and traffics across synaptic boutons. *Cell*. 172:262–274.e11. https://doi.org/10.1016/j.cell.2017.12.022

Ataman, B., J. Ashley, M. Gorczyca, P. Ramachandran, W. Fouquet, S.J. Sigrist, and V. Budnik. 2008. Rapid activity-dependent modifications in synaptic structure and function require bidirectional Wnt signaling. *Neuron*. 57:705–718. https://doi.org/10.1016/j.neuron.2008.01.026

Bao, H., R.W. Daniels, G.T. MacLeod, M.P. Charlton, H.L. Atwood, and B. Zhang. 2005. AP180 maintains the distribution of synaptic and vesicle proteins in the nerve terminal and indirectly regulates the efficacy of Ca^{2+}-triggered exocytosis. *J. Neurophysiol.* 94:1888–1903. https://doi.org/10.1152/jn.00080.2005

Barber, C.F., R.A. Jorquera, J.E. Melom, and J.T. Littleton. 2009. Postsynaptic regulation of synaptic plasticity by synaptotagmin 4 requires both C2 domains. *J. Cell Biol.* 187:295–310. https://doi.org/10.1083/jcb.200903098

Bartscherer, K., N. Pelte, D. Ingelfinger, and M. Boutros. 2006. Secretion of Wnt Ligands Requires Evi, a Conserved Transmembrane Protein. *Cell.* 125:523–533. https://doi.org/10.1016/j.cell.2006.04.009

Becot, A., C. Volgers, and G. van Niel. 2020. Transmissible endosomal intoxication: A balance between exosomes and lysosomes at the basis of intercellular amyloid propagation. *Biomedicines.* 8:272. https://doi.org/10.3390/biomedicines8080272

Bendris, N., and S.L. Schmid. 2017. Endocytosis, metastasis and beyond: Multiple facets of SNX9. *Trends Cell Biol.* 27:189–200. https://doi.org/10.1016/j.tcb.2016.11.001

Blanchette, C.R., and A.A. Rodal. 2020. Mechanisms for biogenesis and release of neuronal extracellular vesicles. *Curr. Opin. Neurobiol.* 63:104–110. https://doi.org/10.1016/j.conb.2020.03.013

Budnik, V., Y.-H. Koh, B. Guan, B. Hartmann, C. Hough, D. Woods, and M. Gorczyca. 1996. Regulation of Synapse Structure and Function by the *Drosophila* Tumor Suppressor Gene dlg. *Neuron.* 17(4):627–640. https://doi.org/10.1016/s0896-6273(00)80196-8

Budnik, V., C. Ruiz-Canada, and F. Wendler. 2016. Extracellular vesicles round off communication in the nervous system. *Nat. Rev. Neurosci.* 17:160–172. https://doi.org/10.1038/nrn.2015.29

Burrinha, T., I. Martinsson, R. Gomes, A.P. Terrasso, G.K. Gouras, and C.G. Almeida. 2021. Up-regulation of APP endocytosis by neuronal aging drives amyloid dependent-synapse loss. *J. Cell Sci.* 134:jcs.255752. https://doi.org/10.1242/jcs.255752

Cao, H., X. Yin, Y. Cao, Y. Jin, S. Wang, Y. Kong, Y. Chen, J. Gao, S. Heller, and Z. Xu. 2013. FCHSD1 and FCHSD2 are expressed in hair cell stereocilia and cuticular plate and regulate actin polymerization in vitro. *PLoS One.* 8:e56516. https://doi.org/10.1371/journal.pone.0056516

Chakraborty, R., V. Vepuri, S.D. Mhatre, B.E. Paddock, S. Miller, S.J. Michelson, R. Delvadia, A. Desai, M. Vinokur, D.J. Melicharek, et al. 2011. Characterization of a *Drosophila* Alzheimer's disease model: Pharmacological rescue of cognitive defects. *PLoS One.* 6:e20799. https://doi.org/10.1371/journal.pone.0020799

Chanaday, N.L., M.A. Cousin, I. Milosevic, S. Watanabe, and J.R. Morgan. 2019. The synaptic vesicle cycle revisited: New insights into the modes and mechanisms. *J. Neurosci.* 39:8209–8216. https://doi.org/10.1523/JNEUROSCI.1158-19.2019

Chen, Z., and S.L. Schmid. 2020. Evolving models for assembling and shaping clathrin-coated pits. *J. Cell Biol.* 219:e202005126. https://doi.org/10.1083/jcb.202005126

Choudhury, S.D., Z. Mushtaq, S. Reddy-Alla, S.S. Balakrishnan, R.S. Thakur, K.S. Krishnan, P. Raghu, M. Ramaswami, and V. Kumar. 2016. σ2-adaptin facilitates basal synaptic transmission and is required for regenerating endo-exo cycling pool under high-frequency nerve stimulation in *Drosophila*. *Genetics.* 203:369–385. https://doi.org/10.1534/genetics.115.183863

Coyle, I.P., Y.H. Koh, W.C.M. Lee, J. Slind, T. Fergestad, J.T. Littleton, and B. Ganetzky. 2004. Nervous wreck, an SH3 adaptor protein that interacts with Wsp, regulates synaptic growth in *Drosophila*. *Neuron.* 41:521–534. https://doi.org/10.1016/s0896-6273(04)00016-9

Daniels, R.W., M.V. Gelfand, C.A. Collins, and A. DiAntonio. 2008. Visualizing glutamatergic cell bodies and synapses in *Drosophila* larval and adult CNS. *J. Comp. Neurol.* 508:131–152. https://doi.org/10.1002/cne.21670

Del Signore, S.J., C.F. Kelley, E.M. Messelaar, T. Lemos, M.F. Marchan, B. Ermanoska, M. Mund, T.G. Fai, M. Kaksonen, and A.A. Rodal. 2021. An autoinhibitory clamp of actin assembly constrains and directs synaptic endocytosis. *Elife.* 10:e69597. https://doi.org/10.7554/eLife.69597

Deshpande, M., Z. Feiger, A.K. Shilton, C.C. Luo, E. Silverman, and A.A. Rodal. 2016. Role of BMP receptor traffic in synaptic growth defects in an ALS model. *Mol. Biol. Cell.* 27:2898–2910. https://doi.org/10.1091/mbc.e16-07-0519

Deshpande, M., and A.A. Rodal. 2016. The crossroads of synaptic growth signaling, membrane traffic, and neurological disease: Insights from *Drosophila*. *Traffic.* 17:87–101. https://doi.org/10.1111/tra.12345

Dickman, D.K., J.A. Horne, I.A. Meinertzhagen, and T.L. Schwarz. 2005. A slowed classical pathway rather than kiss-and-run mediates endocytosis at synapses lacking synaptojanin and endophilin. *Cell.* 123:521–533. https://doi.org/10.1016/j.cell.2005.09.026

Dickman, D.K., Z. Lu, I.A. Meinertzhagen, and T.L. Schwarz. 2006. Altered synaptic development and active zone spacing in endocytosis mutants. *Curr. Biol.* 16:591–598. https://doi.org/10.1016/j.cub.2006.02.058

Dietzl, G., D. Chen, F. Schnorrer, K.-C. Su, Y. Barinova, M. Fellner, B. Gasser, K. Kinsey, S. Oppel, S. Scheiblauer, et al. 2007. A genome-wide transgenic RNAi library for conditional gene inactivation in *Drosophila*. *Nature.* 448:151–156. https://doi.org/10.1038/nature05954

Dwivedi, M.K., S.D. Choudhury, A. Patnaik, S. Mishra, R. Padinjat, and V. Kumar. 2021. AP2 regulates Thickveins trafficking through Rab11 to attenuate NMJ growth signaling in *Drosophila*. *bioRxiv*. https://doi.org/10.1101/2021.01.28.428584

Escudero, C.A., O.M. Lazo, C. Galleguillos, J.I. Parraguez, M.A. Lopez-Verrilli, C. Cabeza, L. Leon, U. Saeed, C. Retamal, A. Gonzalez, et al. 2014. The p75 neurotrophin receptor evades the endolysosomal route in neuronal cells, favouring multivesicular bodies specialised for exosomal release. *J. Cell Sci.* 127:1966–1979. https://doi.org/10.1242/jcs.141754

Farfel-Becker, T., J.C. Roney, X.T. Cheng, S. Li, S.R. Cuddy, and Z.H. Sheng. 2019. Neuronal soma-derived degradative lysosomes are continuously delivered to distal axons to maintain local degradation capacity. *Cell Rep.* 28:51–64.e4. https://doi.org/10.1016/j.celrep.2019.06.013

Feng, Y., A. Ueda, and C.F. Wu. 2004. A modified minimal hemolymph-like solution, HL3.1, for physiological recordings at the neuromuscular junctions of normal and mutant *Drosophila* larvae. *J. Neurogenet.* 18:377–402. https://doi.org/10.1080/01677060490894522

Ferguson, S.M. 2018. Axonal transport and maturation of lysosomes. *Curr. Opin. Neurobiol.* 51:45–51. https://doi.org/10.1016/j.conb.2018.02.020

Fuentes-Medel, Y., M.A. Logan, J. Ashley, B. Ataman, V. Budnik, and M.R. Freeman. 2009. Glia and muscle sculpt neuromuscular arbors by engulfing destabilized synaptic boutons and shed presynaptic debris. *PLoS Biol.* 7:e1000184. https://doi.org/10.1371/journal.pbio.1000184

Gonzalez-Gaitan, M., and H. Jackle. 1997. Role of *Drosophila* alpha-adaptin in presynaptic vesicle recycling. *Cell.* 88:767–776. https://doi.org/10.1016/s0092-8674(00)81923-6

Greeve, I., D. Kretzschmar, J.A. Tschape, A. Beyn, C. Brellinger, M. Schweizer, R.M. Nitsch, and R. Reifegerste. 2004. Age-dependent neurodegeneration and Alzheimer-amyloid plaque formation in transgenic *Drosophila*. *J. Neurosci.* 24:3899–3906. https://doi.org/10.1523/jneurosci.0283-04.2004

Gu, M., Q. Liu, S. Watanabe, L. Sun, G. Hollopeter, B.D. Grant, and E.M. Jorgensen. 2013. AP2 hemicomplexes contribute independently to synaptic vesicle endocytosis. *Elife.* 2:e00190. https://doi.org/10.7554/eLife.00190

Harris, K.P., J.T. Littleton, and B.A. Stewart. 2018. Postsynaptic Syntaxin 4 negatively regulates the efficiency of neurotransmitter release. *J. Neurogenet.* 32:221–229. https://doi.org/10.1080/01677063.2018.1501372

Hazelrigg, T., R. Levis, and G.M. Rubin. 1984. Transformation of white locus DNA in *Drosophila*: Dosage compensation, zeste interaction, and position effects. *Cell.* 36:469–481. https://doi.org/10.1016/0092-8674(84)90240-x

Heerssen, H., R.D. Fetter, and G.W. Davis. 2008. Clathrin dependence of synaptic-vesicle formation at the *Drosophila* neuromuscular junction. *Curr. Biol.* 18:401–409. https://doi.org/10.1016/j.cub.2008.02.055

Heisler, F.F., Y. Pechmann, I. Wieser, H.C. Altmeppen, L. Veenendaal, M. Muhia, M. Schweizer, M. Glatzel, S. Krasemann, and M. Kneussel. 2018. Muskelin coordinates PrP(C) lysosome versus exosome targeting and impacts prion disease progression. *Neuron.* 99:1155–1169.e1159. https://doi.org/10.1016/j.neuron.2018.08.010

Holm, M.M., J. Kaiser, and M.E. Schwab. 2018. Extracellular vesicles: Multimodal envoys in neural maintenance and repair. *Trends Neurosci.* 41:360–372. https://doi.org/10.1016/j.tins.2018.03.006

Hortsch, M., A.J. Bieber, N.H. Patel, and C.S. Goodman. 1990. Differential splicing generates a nervous system—Specific form of *drosophila* neuroglian. *Neuron.* 4:697–709. https://doi.org/10.1016/0896-6273(90)90196-m

Hung, C., E. Tuck, V. Stubbs, S.J. van der Lee, C. Aalfs, R. van Spaendonk, P. Scheltens, J. Hardy, H. Holstege, and F.J. Livesey. 2021. SORL1 deficiency in human excitatory neurons causes APP-dependent defects in the endolysosome-autophagy network. *Cell Rep.* 35:109259. https://doi.org/10.1016/j.celrep.2021.109259

Inoshita, T., T. Arano, Y. Hosaka, H. Meng, Y. Umezaki, S. Kosugi, T. Morimoto, M. Koike, H.Y. Chang, Y. Imai, and N. Hattori. 2017. Vps35 in cooperation with LRRK2 regulates synaptic vesicle endocytosis through

the endosomal pathway in *Drosophila*. *Hum. Mol. Genet.* 26:2933–2948. https://doi.org/10.1093/hmg/ddx179

Janvier, K., and J.S. Bonifacino. 2005. Role of the endocytic machinery in the sorting of lysosome-associated membrane proteins. *Mol. Biol. Cell.* 16: 4231–4242. https://doi.org/10.1091/mbc.e05-03-0213

Jin, E.J., F.R. Kiral, M.N. Ozel, L.S. Burchardt, M. Osterland, D. Epstein, H. Wolfenberg, S. Prohaska, and P.R. Hiesinger. 2018. Live observation of two parallel membrane degradation pathways at axon terminals. *Curr. Biol.* 28:1027–1038.e4. https://doi.org/10.1016/j.cub.2018.02.032

Kaempf, N., and T. Maritzen. 2017. Safeguards of neurotransmission: Endocytic adaptors as regulators of synaptic vesicle composition and function. *Front Cell Neurosci.* 11:320. https://doi.org/10.3389/fncel.2017.00320

Kaksonen, M., and A. Roux. 2018. Mechanisms of clathrin-mediated endocytosis. *Nat. Rev. Mol. Cell Biol.* 19:313–326. https://doi.org/10.1038/nrm.2017.132

Kasprowicz, J., S. Kuenen, K. Miskiewicz, R.L.P. Habets, L. Smitz, and P. Verstreken. 2008. Inactivation of clathrin heavy chain inhibits synaptic recycling but allows bulk membrane uptake. *J. Cell Biol.* 182:1007–1016. https://doi.org/10.1083/jcb.200804162

Kasprowicz, J., S. Kuenen, J. Swerts, K. Miskiewicz, and P. Verstreken. 2014. Dynamin photoinactivation blocks Clathrin and alpha-adaptin recruitment and induces bulk membrane retrieval. *J. Cell Biol.* 204:1141–1156. https://doi.org/10.1083/jcb.201310090

Keating, D.J., C. Chen, and M.A. Pritchard. 2006. Alzheimer's disease and endocytic dysfunction: Clues from the down syndrome-related proteins, DSCR1 and ITSN1. *Ageing Res. Rev.* 5:388–401. https://doi.org/10.1016/j.arr.2005.11.001

Kitamoto, T. 2001. Conditional modification of behavior in *Drosophila* by targeted expression of a temperature-sensitive shibire allele in defined neurons. *J. Neurobiol.* 47:81–92. https://doi.org/10.1002/neu.1018

Kittelmann, M., J.F. Liewald, J. Hegermann, C. Schultheis, M. Brauner, W. Steuer Costa, S. Wabnig, S. Eimer, and A. Gottschalk. 2013. In vivo synaptic recovery following optogenetic hyperstimulation. *Proc. Natl. Acad. Sci. USA.* 110:E3007–E3016. https://doi.org/10.1073/pnas.1305679110

Knaevelsrud, H., K. Soreng, C. Raiborg, K. Haberg, F. Rasmuson, A. Brech, K. Liestol, T.E. Rusten, H. Stenmark, T.P. Neufeld, et al. 2013. Membrane remodeling by the PX-BAR protein SNX18 promotes autophagosome formation. *J. Cell Biol.* 202:331–349. https://doi.org/10.1083/jcb.201205129

Koh, T.W., P. Verstreken, and H.J. Bellen. 2004. Dap160/intersectin acts as a stabilizing scaffold required for synaptic development and vesicle endocytosis. *Neuron.* 43:193–205. https://doi.org/10.1016/j.neuron.2004.06.029

Koles, K., J. Nunnari, C. Korkut, R. Barria, C. Brewer, Y. Li, J. Leszyk, B. Zhang, and V. Budnik. 2012. Mechanism of evenness interrupted (Evi)-exosome release at synaptic boutons. *J. Biol. Chem.* 287:16820–16834. https://doi.org/10.1074/jbc.M112.342667

Kononenko, N.L., D. Puchkov, G. Classen, G.A. Classen, A.M. Walter, A. Pechstein, L. Sawade, N. Kaempf, T. Trimbuch, D. Lorenz, et al. 2014. Clathrin/AP-2 mediate synaptic vesicle reformation from endosome-like vacuoles but are not essential for membrane retrieval at central synapses. *Neuron.* 82:981–988. https://doi.org/10.1016/j.neuron.2014.05.007

Korkut, C., B. Ataman, P. Ramachandran, J. Ashley, R. Barria, N. Gherbesi, and V. Budnik. 2009. Trans-synaptic transmission of vesicular Wnt signals through Evi/Wntless. *Cell.* 139:393–404. https://doi.org/10.1016/j.cell.2009.07.051

Korkut, C., Y. Li, K. Koles, C. Brewer, J. Ashley, M. Yoshihara, and V. Budnik. 2013. Regulation of postsynaptic retrograde signaling by presynaptic exosome release. *Neuron.* 77:1039–1046. https://doi.org/10.1016/j.neuron.2013.01.013

Korolchuk, V.I., M.M. Schutz, C. Gomez-Llorente, J. Rocha, N.R. Lansu, S.M. Collins, Y.P. Wairkar, I.M. Robinson, and C.J. O'Kane. 2007. *Drosophila* Vps35 function is necessary for normal endocytic trafficking and actin cytoskeleton organisation. *J. Cell Sci.* 120:4367–4376. https://doi.org/10.1242/jcs.012336

Lau, A.W., and M.M. Chou. 2008. The adaptor complex AP-2 regulates post-endocytic trafficking through the non-clathrin Arf6-dependent endocytic pathway. *J. Cell Sci.* 121:4008–4017. https://doi.org/10.1242/jcs.033522

Lauwers, E., Y.C. Wang, R. Gallardo, R. Van der Kant, E. Michiels, J. Swerts, P. Baatsen, S.S. Zaiter, S.R. McAlpine, N.V. Gounko, et al. 2018. Hsp90 mediates membrane deformation and exosome release. *Mol. Cell.* 71: 689–702.e9. https://doi.org/10.1016/j.molcel.2018.07.016

Lie, P.P.Y., D.S. Yang, P. Stavrides, C.N. Goulbourne, P. Zheng, P.S. Mohan, A.M. Cataldo, and R.A. Nixon. 2021. Post-Golgi carriers, not lysosomes, confer lysosomal properties to pre-degradative organelles in normal and dystrophic axons. *Cell Rep.* 35:109034. https://doi.org/10.1016/j.celrep.2021.109034

Lin, J.J. 1981. Monoclonal antibodies against myofibrillar components of rat skeletal muscle decorate the intermediate filaments of cultured cells. *Proc. Natl. Acad. Sci. U.S.A.* 78:2335–2339. https://doi.org/10.1073/pnas.78.4.2335

Lin, D.M., and C.S. Goodman. 1994. Ectopic and increased expression of fasciclin II alters motoneuron growth cone guidance. *Neuron.* 13: 507–523. https://doi.org/10.1016/0896-6273(94)90022-1

Littleton, J.T., H.J. Bellen, and M.S. Perin. 1993. Expression of synaptotagmin in *Drosophila* reveals transport and localization of synaptic vesicles to the synapse. *Development.* 118:1077–1088. https://doi.org/10.1242/dev.118.4.1077

Malakooti, N., M.A. Pritchard, F. Chen, Y. Yu, C. Sgambelloni, P.A. Adlard, and D.I. Finkelstein. 2020. The long isoform of intersectin-1 has a role in learning and memory. *Front. Behav. Neurosci.* 14:24. https://doi.org/10.3389/fnbeh.2020.00024

Marie, B., S.T. Sweeney, K.E. Poskanzer, J. Roos, R.B. Kelly, and G.W. Davis. 2004. Dap160/intersectin scaffolds the periactive zone to achieve high-fidelity endocytosis and normal synaptic growth. *Neuron.* 43:207–219. https://doi.org/10.1016/j.neuron.2004.07.001

Merdes, G., P. Soba, A. Loewer, M.V. Bilic, K. Beyreuther, and R. Paro. 2004. Interference of human and *Drosophila* APP and APP-like proteins with PNS development in *Drosophila*. *EMBO J.* 23:4082–4095. https://doi.org/10.1038/sj.emboj.7600413

Mhatre, S.D., V. Satyasi, M. Killen, B.E. Paddock, R.D. Moir, A.J. Saunders, and D.R. Marenda. 2014. Synaptic abnormalities in a *Drosophila* model of Alzheimer's disease. *Dis. Model. Mech.* 7:373–385. https://doi.org/10.1242/dmm.012104

Milosevic, I., S. Giovedi, X. Lou, A. Raimondi, C. Collesi, H. Shen, S. Paradise, E. O'Toole, S. Ferguson, O. Cremona, and P. De Camilli. 2011. Recruitment of endophilin to clathrin-coated pit necks is required for efficient vesicle uncoating after fission. *Neuron.* 72:587–601. https://doi.org/10.1016/j.neuron.2011.08.029

O'Connor-Giles, K.M., L.L. Ho, and B. Ganetzky. 2008. Nervous wreck interacts with thickveins and the endocytic machinery to attenuate retrograde BMP signaling during synaptic growth. *Neuron.* 58:507–518. https://doi.org/10.1016/j.neuron.2008.03.007

Pan, C.L., P.D. Baum, M. Gu, E.M. Jorgensen, S.G. Clark, and G. Garriga. 2008. *C. elegans* AP-2 and retromer control Wnt signaling by regulating mig-14/Wntless. *Dev. Cell.* 14:132–139. https://doi.org/10.1016/j.devcel.2007.12.001

Parks, A.L., K.R. Cook, M. Belvin, N.A. Dompe, R. Fawcett, K. Huppert, L.R. Tan, C.G. Winter, K.P. Bogart, J.E. Deal, et al. 2004. Systematic generation of high-resolution deletion coverage of the *Drosophila* melanogaster genome. *Nat Genet.* 36(3):288–292. https://doi.org/10.1038/ng1312

Parnas, D., A.P. Haghighi, R.D. Fetter, S.W. Kim, and C.S. Goodman. 2001. Regulation of Postsynaptic Structure and Protein Localization by the Rho-Type Guanine Nucleotide Exchange Factor dPix. *Neuron.* 32: 415–424. https://doi.org/10.1016/s0896-6273(01)00485-8

Patel, N.H., B.G. Condron, and K. Zinn. 1994. Pair-rule expression patterns of even-skipped are found in both short- and long-germ beetles. *Nature.* 367:429–434. https://doi.org/10.1038/367429a0

Perkins, L.A., L. Holderbaum, R. Tao, Y. Hu, R. Sopko, K. McCall, D. Yang-Zhou, I. Flockhart, R. Binari, H.-S. Shim, et al. 2015. The Transgenic RNAi Project at Harvard Medical School: Resources and Validation. *Genetics.* 201:843–852. https://doi.org/10.1534/genetics.115.180208

Piccioli, Z.D., and J.T. Littleton. 2014. Retrograde BMP signaling modulates rapid activity-dependent synaptic growth via presynaptic LIM kinase regulation of cofilin. *J. Neurosci.* 34:4371–4381. https://doi.org/10.1523/JNEUROSCI.4943-13.2014

Port, F., M. Kuster, P. Herr, E. Furger, C. Bänziger, G. Hausmann, and K. Basler. 2008. Wingless secretion promotes and requires retromer-dependent cycling of Wntless. *Nat Cell Biol.* 10:178–185. https://doi.org/10.1038/ncb1687

Raiborg, C., K.G. Bache, A. Mehlum, E. Stang, and H. Stenmark. 2001. Hrs recruits clathrin to early endosomes. *EMBO J.* 20:5008–5021. https://doi.org/10.1093/emboj/20.17.5008

Raiborg, C., J. Wesche, L. Malerod, and H. Stenmark. 2006. Flat clathrin coats on endosomes mediate degradative protein sorting by scaffolding Hrs in dynamic microdomains. *J. Cell Sci.* 119:2414–2424. https://doi.org/10.1242/jcs.02978

Ren, Y., H.W. Xu, F. Davey, M. Taylor, J. Aiton, P. Coote, F. Fang, J. Yao, D. Chen, J.X. Chen, et al. 2008. Endophilin I expression is increased in the brains of Alzheimer disease patients. *J. Biol. Chem.* 283:5685–5691. https://doi.org/10.1074/jbc.M707932200

Rodal, A.A., R.N. Motola-Barnes, and J.T. Littleton. 2008. Nervous Wreck and Cdc42 cooperate to regulate endocytic actin assembly during synaptic growth. *J. Neurosci.* 28:8316–8325. https://doi.org/10.1523/JNEUROSCI.2304-08.2008

Sachse, M., S. Urbe, V. Oorschot, G.J. Strous, and J. Klumperman. 2002. Bilayered clathrin coats on endosomal vacuoles are involved in protein sorting toward lysosomes. *Mol. Biol. Cell.* 13:1313–1328. https://doi.org/10.1091/mbc.01-10-0525

Shi, A., L. Sun, R. Banerjee, M. Tobin, Y. Zhang, and B.D. Grant. 2009. Regulation of endosomal clathrin and retromer-mediated endosome to Golgi retrograde transport by the J-domain protein RME-8. *EMBO J.* 28:3290–3302. https://doi.org/10.1038/emboj.2009.272

Smith, R.B., J.B. Machamer, N.C. Kim, T.S. Hays, and G. Marques. 2012. Relay of retrograde synaptogenic signals through axonal transport of BMP receptors. *J. Cell Sci.* 125:3752–3764. https://doi.org/10.1242/jcs.094292

Snow, P.M., N.H. Patel, A.L. Harrelson, and C.S. Goodman. 1987. Neural-specific carbohydrate moiety shared by many surface glycoproteins in *Drosophila* and grasshopper embryos. *J. Neurosci.* 7:4137–4144

Song, Z., Y. Xu, W. Deng, L. Zhang, H. Zhu, P. Yu, Y. Qu, W. Zhao, Y. Han, and C. Qin. 2020. Brain derived exosomes are a double-edged sword in Alzheimer's disease. *Front. Mol. Neurosci.* 13:79. https://doi.org/10.3389/fnmol.2020.00079

Stewart, B.A., H.L. Atwood, J.J. Renger, J. Wang, and C.F. Wu. 1994. Improved stability of *Drosophila* larval neuromuscular preparations in haemolymph-like physiological solutions. *J. Comp. Physiol. A.* 175:179–191. https://doi.org/10.1007/BF00215114

Sweeney, S.T., and G.W. Davis. 2002. Unrestricted synaptic growth in spinster-a late endosomal protein implicated in TGF-beta-mediated synaptic growth regulation. *Neuron.* 36:403–416. https://doi.org/10.1016/s0896-6273(02)01014-0

Ukken, F.P., J.J. Bruckner, K.L. Weir, S.J. Hope, S.L. Sison, R.M. Birschbach, L. Hicks, K.L. Taylor, E.W. Dent, G.B. Gonsalvez, and K.M. O'Connor-Giles. 2016. BAR-SH3 Sorting nexins are conserved Nervous wreck interactors that organize synapses and promote neurotransmission. *J. Cell Sci.* 129:166–177. https://doi.org/10.1242/jcs.178699

Moline, M.M., C. Southern, and A. Bejsovec. 1999. Directionality of wingless protein transport influences epidermal patterning in the *Drosophila* embryo. *Development.* 126:4375–4384. https://doi.org/10.1242/dev.126.19.4375

van Niel, G., G. D'Angelo, and G. Raposo. 2018. Shedding light on the cell biology of extracellular vesicles. *Nat. Rev. Mol. Cell Biol.* 19:213–228. https://doi.org/10.1038/nrm.2017.125

Verstreken, P., T.-W. Koh, K.L. Schulze, R.G. Zhai, P.R. Hiesinger, Y. Zhou, S.Q. Mehta, Y. Cao, J. Roos, and H.J. Bellen. 2003. Synaptojanin Is Recruited by Endophilin to Promote Synaptic Vesicle Uncoating. *Neuron.* 40:733–748. https://doi.org/10.1016/s0896-6273(03)00644-5

Verstreken, P., O. Kjaerulff, T.E. Lloyd, R. Atkinson, Y. Zhou, I.A. Meinertzhagen, and H.J. Bellen. 2002. Endophilin mutations block clathrin-mediated endocytosis but not neurotransmitter release. *Cell.* 109:101–112. https://doi.org/10.1016/s0092-8674(02)00688-8

Walsh, R.B., E.C. Dresselhaus, A.N. Becalska, M.J. Zunitch, C.R. Blanchette, A.L. Scalera, T. Lemos, S.M. Lee, J. Apiki, S. Wang, et al. 2021. Opposing functions for retromer and Rab11 in extracellular vesicle traffic at presynaptic terminals. *J. Cell Biol.* 220.e202012034. https://doi.org/10.1083/jcb.202012034

Watanabe, S., T. Trimbuch, M. Camacho-Perez, B.R. Rost, B. Brokowski, B. Sohl-Kielczynski, A. Felies, M.W. Davis, C. Rosenmund, and E.M. Jorgensen. 2014. Clathrin regenerates synaptic vesicles from endosomes. *Nature.* 515:228–233. https://doi.org/10.1038/nature13846

Wenzel, E.M., S.W. Schultz, K.O. Schink, N.M. Pedersen, V. Nahse, A. Carlson, A. Brech, H. Stenmark, and C. Raiborg. 2018. Concerted ESCRT and clathrin recruitment waves define the timing and morphology of intraluminal vesicle formation. *Nat. Commun.* 9:2932. https://doi.org/10.1038/s41467-018

West, R.J.H., Y. Lu, B. Marie, F.-B. Gao, and S.T. Sweeney. 2015. Rab8, POSH, and TAK1 regulate synaptic growth in a *Drosophila* model of frontotemporal dementia. *Journal of Cell Biology.* 208:931–947. https://doi.org/10.1083/jcb.201404066

Winckler, B., V. Faundez, S. Maday, Q. Cai, C. Guimas Almeida, and H. Zhang. 2018. The endolysosomal system and proteostasis: From development to degeneration. *J. Neurosci.* 38:9364–9374. https://doi.org/10.1523/JNEUROSCI.1665-18.2018

Windler, S.L., and D. Bilder. 2010. Endocytic Internalization Routes Required for Delta/Notch Signaling. *Current Biology.* 20:538–543. https://doi.org/10.1016/j.cub.2010.01.049

Wong, M.Y., S.L. Cavolo, and E.S. Levitan. 2015. Synaptic neuropeptide release by dynamin-dependent partial release from circulating vesicles. *Mol. Biol. Cell.* 26:2466–2474. https://doi.org/10.1091/mbc.E15-01-0002

Xiao, G.Y., A. Mohanakrishnan, and S.L. Schmid. 2018. Role for ERK1/2-dependent activation of FCHSD2 in cancer cell-selective regulation of clathrin-mediated endocytosis. *Proc. Natl. Acad. Sci. USA.* 115:E9570–E9579. https://doi.org/10.1073/pnas.1810209115

Xiao, G.Y., and S.L. Schmid. 2020. FCHSD2 controls oncogenic ERK1/2 signaling outcome by regulating endocytic trafficking. *PLoS Biol.* 18–e3000778. https://doi.org/10.1371/journal.pbio.3000778

Xiao, Q., P. Yan, X. Ma, H. Liu, R. Perez, A. Zhu, E. Gonzales, D.L. Tripoli, L. Czerniewski, A. Ballabio, et al. 2015. Neuronal-targeted TFEB accelerates lysosomal degradation of APP, reducing Aβ generation and amyloid plaque pathogenesis. *J. Neurosci.* 35:12137–12151. https://doi.org/10.1523/JNEUROSCI.0705-15.2015

Yang, P.T., M.J. Lorenowicz, M. Silhankova, D.Y. Coudreuse, M.C. Betist, and H.C. Korswagen. 2008. Wnt signaling requires retromer-dependent recycling of MIG-14/Wntless in Wnt-producing cells. *Dev. Cell.* 14:140–147. https://doi.org/10.1016/j.devcel.2007.12.004

Yarwood, R., J. Hellicar, P.G. Woodman, and M. Lowe. 2020. Membrane trafficking in health and disease. *Dis. Model. Mech.* 13:dmm043448. https://doi.org/10.1242/dmm.043448

Yoshihara, M., B. Adolfsen, K.T. Galle, and J.T. Littleton. 2005. Retrograde signaling by Syt 4 induces presynaptic release and synapse-specific growth. *Science.* 310:858–863. https://doi.org/10.1126/science.1117541

Yu, Q., Y. Wang, F. Du, S. Yan, G. Hu, N. Origlia, G. Rutigliano, Q. Sun, H. Yu, J. Ainge, et al. 2018. Overexpression of endophilin A1 exacerbates synaptic alterations in a mouse model of Alzheimer's disease. *Nat. Commun.* 9:2968. https://doi.org/10.1038/s41467-018-04389-0

Zhang, P., A.N. Holowatyj, T. Roy, S.M. Pronovost, M. Marchetti, H. Liu, C.M. Ulrich, and B.A. Edgar. 2019. An SH3PX1-dependent endocytosis-autophagy network restrains intestinal stem cell proliferation by counteracting EGFR-ERK signaling. *Dev. Cell.* 49:574–589.e5. https://doi.org/10.1016/j.devcel.2019.03.029

Zhu, L., M. Zhong, J. Zhao, H. Rhee, I. Caesar, E.M. Knight, L. Volpicelli-Daley, V. Bustos, W. Netzer, L. Liu, et al. 2013. Reduction of synaptojanin 1 accelerates Abeta clearance and attenuates cognitive deterioration in an Alzheimer mouse model. *J. Biol. Chem.* 288:32050–32063. https://doi.org/10.1074/jbc.m113.504365

JCB

Supplemental material

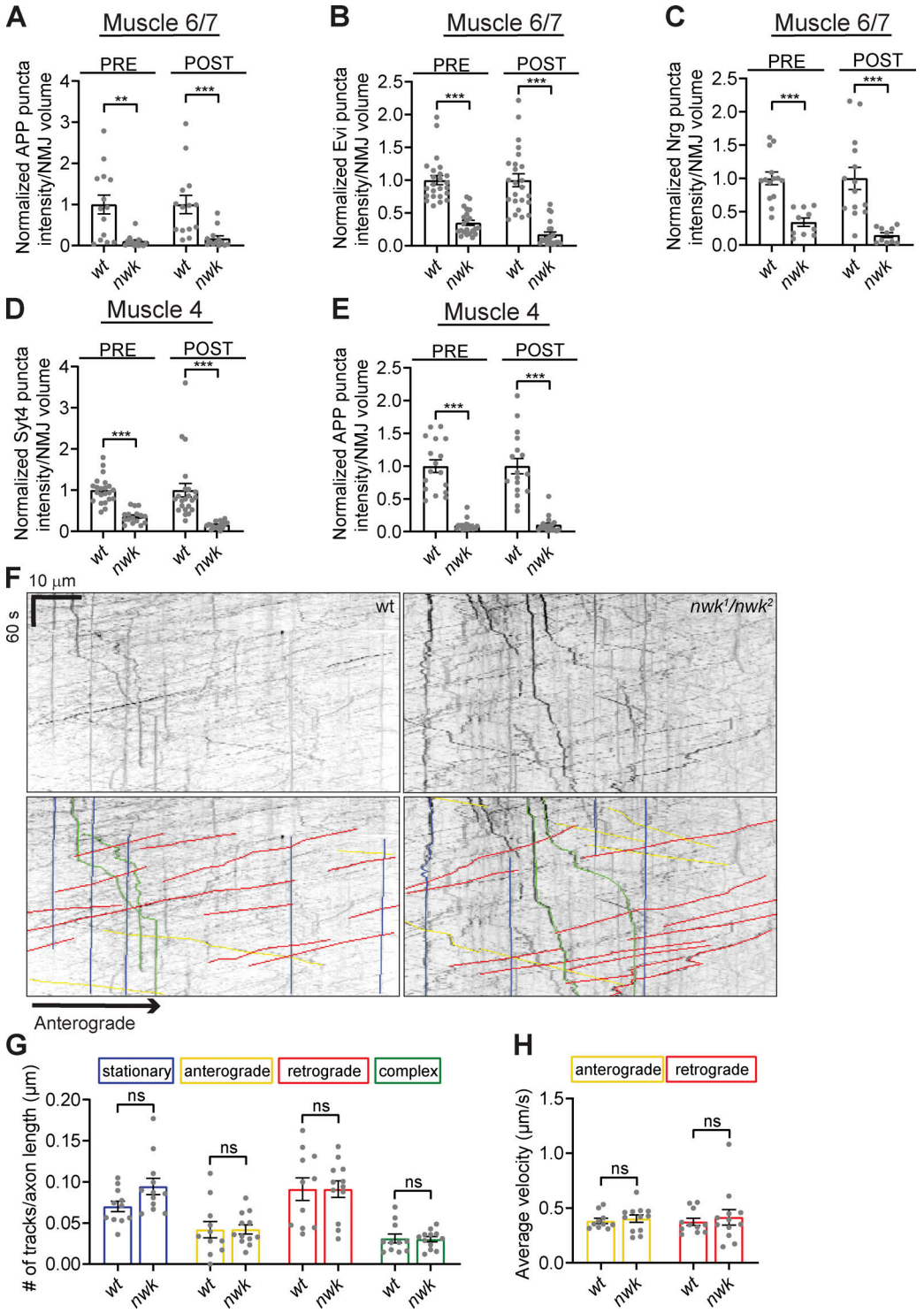

Figure S1. **EV cargo levels are reduced at *nwk* mutant synaptic terminals but show no change in axonal trafficking. (A–E)** Fig. 1 C datasets shown with corresponding controls. **(A)** Quantification of APP-GFP pre- and postsynaptic puncta intensity at muscle 6/7 NMJs. **(B)** Quantification of Evi-GFP pre- and postsynaptic puncta intensity at muscle 6/7 NMJs. **(C)** Quantification of Nrg pre and postsynaptic puncta intensity at muscle 6/7 NMJs. **(D)** Quantification of Syt4-GFP pre- and postsynaptic puncta intensity at muscle 4 NMJs. **(E)** Quantification of APP-GFP pre- and postsynaptic puncta intensity at muscle 4 NMJs. **(F)** Top: Representative kymographs of APP-GFP puncta dynamics in control and *nwk* mutant live axons. Bottom: Overlayed colored lines indicate stationary (blue), anterograde (yellow), retrograde (red), and complex (green) APP-GFP tracks. **(G)** Quantification of number of stationary (blue), anterograde (yellow), retrograde (red), and complex (green) APP-GFP puncta tracks in control and *nwk* mutant axons. **(H)** Quantification of average velocity of anterograde (yellow) and retrograde (red) APP-GFP puncta movement in control and *nwk* mutant axons. Data is represented as mean ± SEM; *n* is depicted by individual gray dots on the graphs and represents NMJs (A–E) and animals (G and H). NMJ intensity measurements were normalized to presynaptic volume (A–E). Number of tracks were normalized to axon length (G). Measurements in A–E were further normalized to the mean of their respective controls. Associated with Fig. 1. See Table S1 and Table S3 for detailed genotypes, sample sizes, and statistical analyses. wt, wild-type.

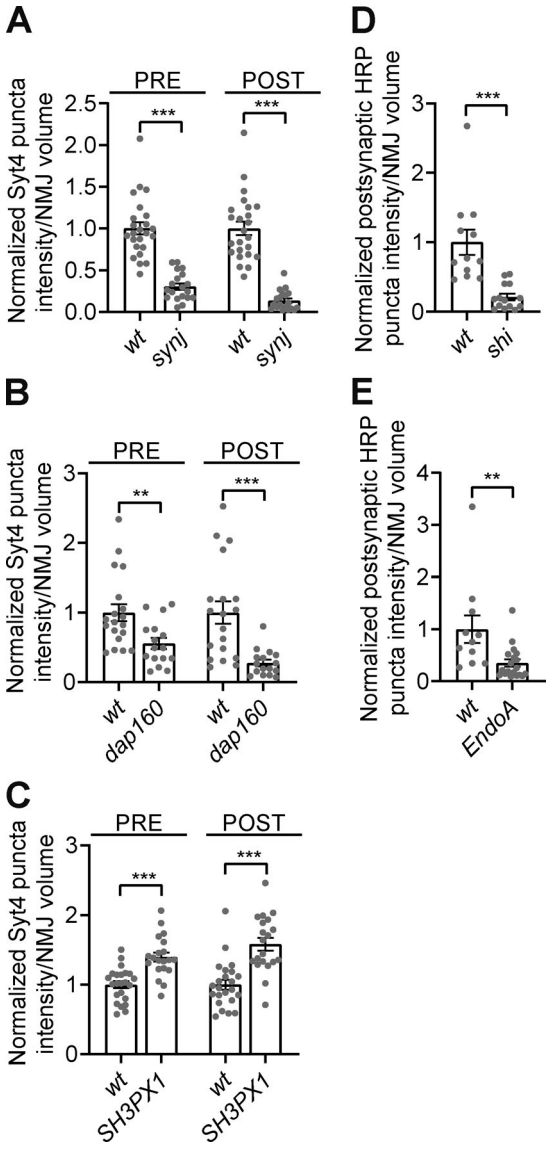

Figure S2. **A subset of endocytic machinery is required for synaptic EV traffic.** Fig. 3, A and B datasets shown with corresponding controls. **(A)** Quantification of pre- postsynaptic Syt4-GFP puncta intensity in control (wt) and *synj* mutants. **(B)** Quantification of pre- and postsynaptic Sy4-GFP puncta intensity in control and upon neuronal knockdown of *dap160*. **(C)** Quantification of pre- and postsynaptic Syt4-GFP puncta intensity in control and *SH3PX1* mutants. **(D)** Quantification of postsynaptic HRP puncta intensity in control and upon neuronal expression of Shi^{K44A}. **(E)** Quantification of postsynaptic HRP puncta intensity in control and upon neuronal knockdown of *EndoA*. Data is represented as mean ± SEM; *n* is depicted by individual gray dots on the graphs and represents NMJs. NMJ intensity measurements were normalized to presynaptic volume; all measurements were further normalized to the mean of their respective controls. Associated with Fig. 3. See Table S1 and Table S3 for detailed genotypes, sample sizes, and statistical analyses.

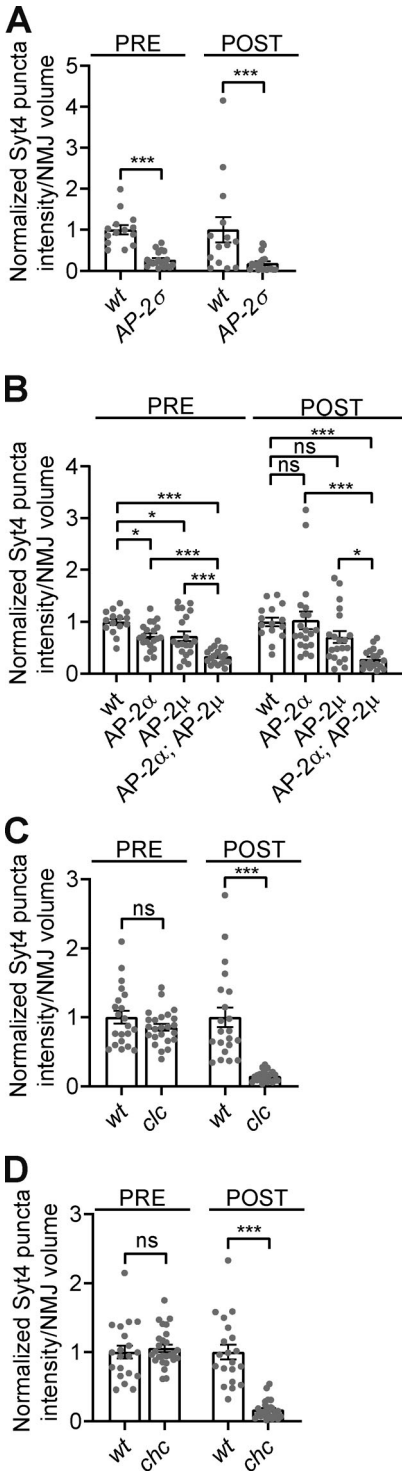

Figure S3. **EV traffic is dependent on clathrin-associated endocytic machinery.** Fig. 4, A and B datasets shown with corresponding controls. **(A)** Quantification of Syt4-GFP pre- and postsynaptic puncta intensity in control (wt) and *AP-2σ* mutants. **(B)** Quantification of Syt4-GFP pre- and postsynaptic puncta intensity in control, *AP-2α*, *AP-2μ*, and *AP-2α;AP-2μ* mutants. **(C)** Quantification of Syt4-GFP pre- and postsynaptic puncta intensity in control and *clc* mutants. **(D)** Quantification of Syt4-GFP pre- and postsynaptic puncta intensity in control and *chc* mutants. Data is represented as mean ± SEM; *n* is depicted by individual gray dots on the graphs and represents NMJs. NMJ intensity measurements were normalized to presynaptic volume; all measurements were further normalized to the mean of their respective controls. Associated with Fig. 4. See Table S1 and Table S3 for detailed genotypes, sample sizes, and statistical analyses.

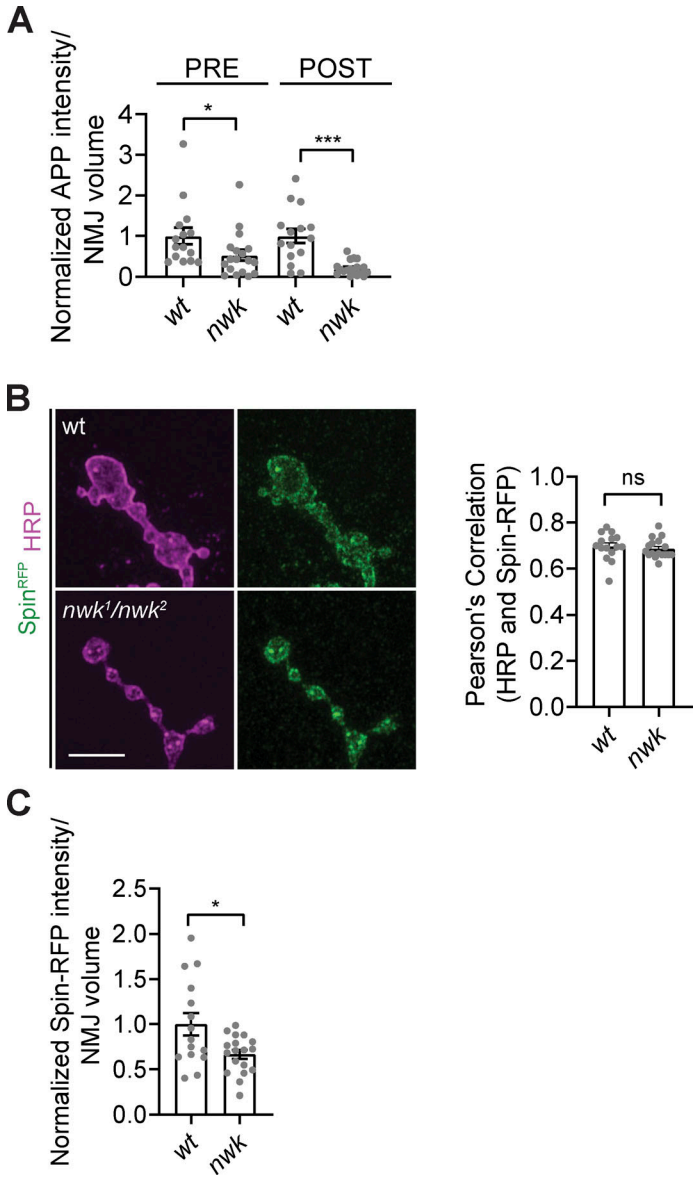

Figure S4. **EV cargo levels are reduced at *nwk* mutant synapses, and remaining EV cargo puncta specifically colocalize with degradative compartments. (A)** Quantification of APP-GFP pre- and postsynaptic puncta intensity in control (wt) and *nwk* mutants. **(B)** Presynaptic α-HRP and Spin-RFP colocalize to the same degree at control and *nwk* mutant NMJs. (Left) Representative Airyscan images of muscle 6/7 NMJs with α-HRP and Spin-RFP. (Right) Pearson's correlation of presynaptic α-HRP and Spin-RFP. **(C)** Quantification of presynaptic Spin-RFP puncta intensity in control and *nwk* mutants. Data is represented as mean ± SEM; *n* is depicted by individual gray dots on the graphs and represents NMJs. NMJ intensity measurements were normalized to presynaptic volume; all measurements were further normalized to the mean of their respective controls. Scale bar is 5 µm. Associated with Fig. 5. See Table S1 and Table S3 for detailed genotypes, sample sizes, and statistical analyses.

Provided online are three tables. Table S1 lists *Drosophila* strains. Table S2 lists antibodies and reagents. Table S3 lists statistics by dataset.